Antibody-secreting cell repertoires hold high-affinity anti-rocuronium specificities that can induce anaphylaxis in vivo

Alice Dejoux, Qianqian Zhu, Adam Woolfe, Ophélie Godon, Sami Ellouze, Guillaume Mottet, Carlos Castrillon, Caitlin M. Gillis, Cyprien Pecalvel, Christelle Ganneau, et al.

Antibody-secreting cell repertoires hold high-affinity anti-rocuronium specificities that can induce anaphylaxis in vivo

Alice Dejoux, PhD, Qianqian Zhu, PhD, Adam Woolfe, PhD, Ophélie Godon, Sami Ellouze, Guillaume Mottet, PhD, Carlos Castrillon, PhD, Caitlin Gillis, PhD, Cyprien Pecalvel, Christelle Ganneau, Bruno Iannascoli, Frédéric Lemoine, PhD, Frederick Saul, PhD, Patrick England, PhD, Laurent L. Reber, PhD, Aurélie Gouel-Chéron, MD, PhD, Luc de Chaisemartin, PharmD, PhD, Ahmed Haouz, PhD, Gaël A. Millot, PhD, Sylvie Bay, PhD, Annabelle Gérard, PhD, Friederike Jönsson, PhD, Sylvie Chollet-Martin, MD, PhD, Pierre Bruhns, PhD

PII: S0091-6749(25)00113-7

DOI: https://doi.org/10.1016/j.jaci.2025.01.025

Reference: YMAI 16658

To appear in: *Journal of Allergy and Clinical Immunology*

Received Date: 30 July 2024

Revised Date: 15 January 2025

Accepted Date: 27 January 2025

Please cite this article as: Dejoux A, Zhu Q, Woolfe A, Godon O, Ellouze S, Mottet G, Castrillon C, Gillis C, Pecalvel C, Ganneau C, Iannascoli B, Lemoine F, Saul F, England P, Reber LL, Gouel-Chéron A, de Chaisemartin L, Haouz A, Millot GA, Bay S, Gérard A, Jönsson F, Chollet-Martin S, Bruhns P, Antibody-secreting cell repertoires hold high-affinity anti-rocuronium specificities that can induce anaphylaxis in vivo, *Journal of Allergy and Clinical Immunology* (2025), doi: https://doi.org/10.1016/j.jaci.2025.01.025.

Antibody-secreting cell repertoires hold high-affinity anti-rocuronium specificities that can induce anaphylaxis in vivo

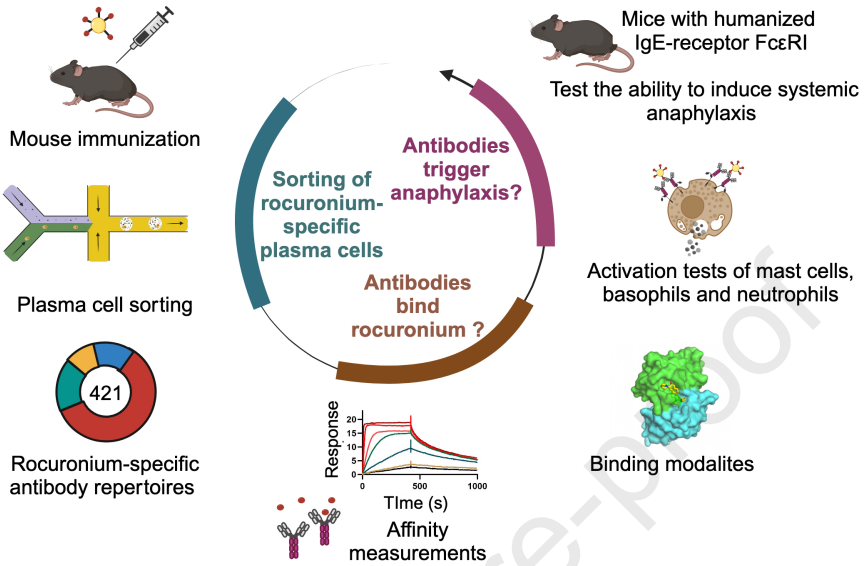

Antibody-secreting cell repertoires hold high-affinity anti-rocuronium specificities that can induce anaphylaxis in vivo

Authors: Alice Dejoux, PhD[1,2,†], Qianqian Zhu, PhD[1,3,†], Adam Woolfe, PhD[4,5,‖], Ophélie Godon[1,‖], Sami Ellouze[4], Guillaume Mottet, PhD[1], Carlos Castrillon, PhD[1], Caitlin Gillis, PhD[1], Cyprien Pecalvel[6], Christelle Ganneau[7], Bruno Iannascoli[1], Frédéric Lemoine, PhD[8], Frederick Saul, PhD[9], Patrick England, PhD[10], Laurent L. Reber, PhD[6], Aurélie Gouel-Chéron, MD, PhD[1,11,12], Luc de Chaisemartin, PharmD, PhD[3,13], Ahmed Haouz, PhD[9], Gaël A. Millot, PhD[1,8], Sylvie Bay, PhD[7], Annabelle Gérard, PhD[4,5,§], Friederike Jönsson, PhD[1,14,§], Sylvie Chollet-Martin, MD, PhD[3,13,§] and Pierre Bruhns, PhD[1,15,§,*].

Affiliations:

[1]Institut Pasteur, Université Paris Cité, INSERM UMR1222, Antibodies in Therapy and Pathology, 75015 Paris, France.

[2]Sorbonne Université, Collège Doctoral, 75005 Paris, France.

[3]Université Paris-Saclay, INSERM, Inflammation Microbiome Immunosurveillance, Orsay, France.

[4]HiFiBiO Therapeutics SAS, Paris, France.

[5]Present address: SABER BIO, Institut du Cerveau, iPEPS The HealthtechHub, 47 boulevard de l'Hôpital CS21414, 75646 Paris Cedex

[6]Toulouse Institute for Infectious and Inflammatory Diseases (Infinity), INSERM UMR1291, CNRS UMR5051, University Toulouse III; Toulouse, France.

[7]Institut Pasteur, Université Paris Cité, CNRS UMR3523, Chimie des Biomolécules, 75015 Paris, France.

[8]Institut Pasteur, Université Paris Cité, Bioinformatics and Biostatistics Hub, Paris, France.

[9]Institut Pasteur, Université Paris Cité, CNRS UMR3528, Plate-forme Cristallographie-C2RT, Paris, France.

[10]Institut Pasteur, Université Paris Cité, CNRS UMR3528, Molecular Biophysics Core Facility, Paris, France.

[11]Anaesthesiology and Critical Care Medicine Department, DMU Parabol, Bichat-Claude Bernard Hospital, AP-HP, 75018 Paris, France.

[12]Université Paris Cité, 75010 Paris, France.

[13]Service d'immunologie, Hôpital Bichat, APHP, Paris, France.

[14]CNRS, F-75015 Paris.

[15]INSERM 1152, DHU FIRE, Labex Inflamex, Université Paris Diderot Paris 7, Paris, France.

[† or ‖]: Equal contribution.

[§]: Co-senior authorship.

*To whom correspondence should be addressed: **Pierre Bruhns**, Unit of Antibodies in Therapy and Pathology, Department of Immunology, Institut Pasteur, 25 rue du Docteur Roux, 75015 Paris, France. Phone: +33-145688629. E-mail: bruhns@pasteur.fr

ABSTRACT

Background: Neuromuscular blocking agents (NMBA) are muscle relaxants used to assist mechanical ventilation but lead in 1/10,000 anesthesia to severe acute hypersensitivity reactions i.e., anaphylaxis. Incidences vary between types of NMBAs. Rocuronium, a widely used non-depolarizing aminosteroid NMBA, induces among the highest anaphylaxis rates. Rocuronium-induced anaphylaxis is proposed to rely on pre-existing rocuronium-binding antibodies, but no such antibodies have ever been identified.

Objectives: Identify rocuronium-specific antibody repertoires from plasma cells or plasmablasts of rocuronium-immunized mice, and determine the affinities, structures and anaphylactogenic potential of these antibodies for rocuronium.

Methods: Herein, we engrafted rocuronium onto carrier proteins allowing immunization of mice against rocuronium, screening for rocuronium-specific antibody responses, and sorting of rocuronium-specific plasma cells using droplet microfluidics coupled to single-cell antibody gene (VH and VL) sequencing.

Results: The two different repertoires of >500 VH-VL pairs were oligoclonal, comprised of three major clonal families, and displayed convergence. Expressed as human IgG1, these antibodies demonstrated subnanomolar affinities for rocuronium with families either monospecific for rocuronium or cross-reactive only for closely-related NMBAs. Expressed as human IgE, they triggered human mast cell and basophil activation, and severe passive systemic anaphylaxis in mice humanized for the IgE receptor FcεRI. Co-crystal structures between rocuronium and antibody representatives of three different VH-VL families revealed distinct interaction modes with, however, the ammonium group involved systematically in the binding interface.

Conclusions: This work identifies the epitopes of antibody reactivity to rocuronium, demonstrates anaphylactogenic potential of anti-rocuronium IgE and establishes the first mouse model of NMBA anaphylaxis.

CAPSULE SUMMARY (35 words)

Immunizing mice with neuromuscular blocking agent rocuronium enabled identification from IgG-secreting cells of rocuronium-specific high affinity antibodies. Expressed as human IgE these antibodies trigger mast cell and basophil activation, and systemic anaphylaxis in mouse models.

KEY MESSAGES

- Generation of plasma cell and plasmablast antibody repertoires that represent circulating antibody pools.
- Identification of the first high-affinity anti-rocuronium antibodies that demonstrate their anaphylactogenic potential.
- Generation of the first animal model of rocuronium anaphylaxis that allows for testing novel drugs.

ABBREVIATIONS

BAT, Basophil Activation Test;
BLI, Bio-layer interferometry;
CDR, Complementary Determining Region;
FcγRs, IgG receptors;
HSA, Human Serum Albumin;
KLH, Keyhole Limpet Hemocyanin;
MAT, Mast cell Activation Test;
NMBAs, Neuromuscular Blocking agents;
PAF, Platelet-activating Factor;
PBMC, peripheral blood mononuclear cells;
QAM, Quaternary Ammonium Molecule;
scFv, single-chain variable fragment;
SPR, Surface Plasmon Resonance;
VH, variable heavy chain;
VHH, Llama single domain antibody or nanobody;
VL, variable light chain.

INTRODUCTION

Neuromuscular Blocking agents (NMBAs) are used in the clinic to paralyze skeletal muscles during surgery conducted under general anesthesia[1, 2]. They help assist airway management in elective or urgent anesthesia by facilitating endotracheal intubation. NMBAs possess two tertiary and/or quaternary substituted ammonium groups at physiological pH that enable them to compete at the neuromuscular junction with the quaternary ammonium group of acetylcholine for binding to muscle-type nicotinic receptors[3].

The most dramatic adverse event following NMBA exposure is anaphylaxis, the severest form of allergic reactions that can lead to death[4, 5]. In some countries, half of perioperative anaphylaxis is caused by NMBAs with a global mortality rate of 4.1%[6]. The current dogma proposes that allergen-specific IgE antibodies, including anti-NMBA IgEs[7], lead to mast cell and basophil activation in allergen-sensitized patients[8]. We reported earlier that, indeed, circulating anti-NMBA IgE levels, but also anti-NMBA IgG levels, correlate with the severity of anaphylaxis[9]. In our view, two antibody-dependent pathways are involved in NMBA-induced anaphylaxis: the IgE pathway leading to mast cell and basophil activation with histamine release as a major mediator, and the IgG pathway leading to neutrophil and monocyte activation with Platelet-activating Factor (PAF) release as a main mediator[8]. Both histamine and PAF induce vasodilation, bronchoconstriction, cardiac and pulmonary failure, with probable cumulative or potentiating effects when both mediators are released. The current treatment relies on adrenaline administration to induce vasoconstriction and bronchodilation, and also antihistamines administered mainly as a safety measure as these are not efficient at controlling anaphylactic shock[10]. Intriguingly, the non-depolarizing aminosteroid NMBA rocuronium can be captured within minutes by the cyclodextrin sugammadex to reverse neuromuscular blockade in patients, leading in a few cases to amelioration of anaphylactic severity[11, 12].

The tertiary and quaternary substituted ammonium groups present in NMBAs have been proposed to be part of the epitope recognized by anti-NMBA antibodies in patients[7], as patient sera reacting with one or several NMBAs[13] cross-react with unrelated molecules possessing a quaternary ammonium[14, 15]. Since anti-NMBA mAbs have never been reported, neither from patients nor animals, molecular or structural evidence is lacking to confirm these hypotheses. Adding complications to the understanding of the allergenic epitope, different conformer species

can coexist. Indeed, rocuronium ring A can adopt a chair or a twist-boat conformation[16], with the twist-boat conformation being favorable for the accommodation of rocuronium within the cyclodextrin sugammadex[17].

Importantly, anaphylaxis occurs at the first exposure to aminosteroid NMBAs in half of the patients[18], excluding NMBAs as primary sensitizing epitopes in these patients' history. In addition, NMBAs are small (molecular weight ≈ 300-1,000 Da) and non-immunogenic. Several families of compounds are however considered to sensitize towards NMBAs, including cough syrups containing pholcodine (a morphine-based compound), cosmetics, cleaning and bleaching products[13, 19-21]. Routinely, anti-NMBA IgEs are quantified using a surrogate for NMBA in ImmunoCAP™ detection: a morphine group termed Quaternary Ammonium Molecule (QAM) that resembles core structures of aminosteroid NMBAs[22, 23]. Large variations in serum reactivity profiles to NMBAs are found between individuals, from a single NMBA to NMBAs belonging to the same chemical family, and even to all NMBAs in 4% of the cases[13]. This suggests B cell responses with one or multiple monospecificities each toward a particular compound, and/or cross-reactive B cell responses towards different NMBAs[7]. Understanding the reason for mono-or cross-reactivity in patients would require analyzing their antibody repertoire and study representative antibodies to determine if cross-reactive mAbs do exist in patients, or rather if a collection of monospecific mAbs targets different NMBAs. The antibody repertoire is classically studied from circulating memory B cells[24, 25], but can also be defined from tissue-resident plasma cells that are proposed to harbor the highest affinity antibodies[26-29].

Rocuronium represents an advantageous study model of NMBA anaphylaxis as it has among the highest anaphylaxis incidences[5, 30-32] and is widely used. In addition, rocuronium possesses a hydroxyl group that can be targeted chemically to allow engraftment on larger molecules for immunization or assay development. In this study, we analyzed the rocuronium-specific antibody repertoires from plasma cells of rocuronium-immunized mice using single cell droplet-based microfluidic technologies[26]. Affinities for rocuronium were in the subnanomolar to nanomolar range with either monospecificity for rocuronium or crossreactivity only to closely related aminosteroid NMBAs that could be explained by crystallographic structures. Anti-rocuronium antibodies were anaphylactogenic when expressed as human IgE *in vitro* and *in vivo* in mice. Identification of anti-rocuronium mAbs allowed to develop the first mouse model of rocuronium anaphylaxis.

METHODS

Mice

C57BL/6J mice were purchased from Charles River, and used for experiments after maintaining the mice for at least one week in SPF conditions after arrival in Institut Pasteur's animal facility. Human FcεRI^{tg} mouse FcεRI$^{-/-}$ mice on the C57BL/6 background were described previously[33]. Mice were bred at Institut Pasteur and used for experiments at 7-12 weeks of age. All animal care and experimentation were conducted in compliance with the guidelines and specific approval of the Animal Ethics committee CETEA number 89 (Institut Pasteur, Paris, France) registered under #170043, #2013-0103 and #27465 and by the French Ministry of Research under agreement #00513.02.

Production and characterization of rocuronium bioconjugates

Hapten-protein couplings were performed using active ester derivatives of rocuronium and KLH or monomeric HSA as the carrier protein. A carboxylate function was first introduced by adding succinic anhydride to rocuronium bromide in the presence of 4-(dimethylamino)-pyridine in pyridine. After stirring overnight at room temperature under argon, the solvent was removed under vacuum. The crude compound was purified by reverse-phase flash chromatography, resulting in a rocuronium derivative with a carboxylic acid (Roc-COOH) at the 3-position of the steroid scaffold. The compound was characterized by mass spectrometry and by nuclear magnetic resonance analysis. All quantities of products were calculated relative to the carrier protein. The functionalized rocuronium (200 equivalent) was dissolved in 0.05 M MES + 0.5 M NaCl buffer (pH 5.6) and combined with 1-ethyl-3-(3-dimethylaminopropyl) carbodiimide (400 equivalent) in the presence of N-hydroxysulfosuccinimide (200 equivalent). After 5-min stirring at room temperature, pH was adjusted to 7.2 with 2 M NaOH. This solution was progressively added to the carrier protein dissolved in 100mM PBS (pH7.2). After 3 hours of gentle agitation at room temperature and buffer exchange in 20mM HEPES et 300mM NaCl with minitrap desalting columns. The exact measurement of the concentration of the bioconjugates was achieved by quantitative amino acid analysis. The average density of conjugated rocuronium derivatives was evaluated by matrix-assisted laser desorption/ionization time-of-flight mass spectrometry. The

HSA-rocuronium conjugates used for all experiments were monomeric with an average engraftment of 32 or 10 rocuronium molecules per HSA molecule for sorting and characterization (ELISA and BLI) experiments, respectively, determined with the mean of the gaussian distribution of the m/z (mass-to-charge ratio) by matrix-assisted laser desorption/ionization time-of-flight mass spectrometry, as we reported earlier[7, 9].

Immunization of mice against rocuronium

Female C57Bl/6J were immunized subcutaneously with 10 μg KLH-rocuronium (or KLH only as control) combined with adjuvant alum 1:1 (v:v) and 20 ng pertussis toxin in physiological saline 0.9% NaCl for three times at 3-week intervals. Mice were boosted with 10 μg KLH-rocuronium without adjuvant three weeks after the last immunization. Four days later, the superficial cervical lymph nodes were removed, and cells resuspended as single cells for immediate sorting using droplet microfluidics.

Plasma cell sorting using droplet microfluidics

Plasma cells and plasmablasts were sorted based on their secretion of IgG antibodies binding to HSA-rocuronium using methods and instruments as we reported earlier[26]. In brief, single cells from lymph nodes of immunized mice were encapsulated into microfluidic droplets with paramagnetic nanoparticles (Strep Plus, 300 nm, Ademtech) coated with biotinylated anti-mouse IgGκ V_HH, 75 nM rabbit $F(ab')_2$ anti-mouse IgG Fc-specific (AlexaFluor647-labeled, Jackson ImmunoResearch) and 50 nM HSA-rocuronium (purified monomer, AlexaFluor488-labeled). Under the influence of a magnetic field, the nanoparticles align into a beadline within each droplet[34] and are flown through a droplet sorting chip placed under a high-speed camera, lasers and PMTs. Relocation of both AlexaFluor647 and FITC fluorescence onto the beadline of one drop triggered sorting of these droplets by dielectrophoresis into a collection tube, followed by cell recovery, re-compartmentalized in droplets with single barcoded hydrogel beads and lysis and reverse transcription reagents using a microfluidic device for subsequent cell lysis and cDNA synthesis. The sequencing library was generated by two-step nested PCR with the barcoded cDNA. Final products were sequenced on an Illumina MiSeq (2x300 bp paired-end reads), which allowed sequencing of the entire VH and VL domain as well as the barcode sequence, as described[26]. A bioinformatics pipeline was developed to allow sequence read trimming, merging, barcode

extraction and clustering, and antibody sequence characterization and filtering. Importantly, for each barcode cluster that contained productive VH and VL made up of at least 20 reads each, the most abundant VH and VL rearrangement were considered to be paired.

Antibody repertoire analysis and representative mAb selection

For reproducibility matters[35], all the bioinformatics analyses of the batches of nucleotide sequence Fasta files, representing the raw single cell Sanger sequencing of the VH-VL IgG domains were implemented in a Nextflow (10.1038/nbt.3820) workflow, with software environment managed by Apptainer (https://apptainer.org). The workflow is available at https://gitlab.pasteur.fr/gmillot/repertoire_profiler, and is detailed below. Most of the process is based on tools from the *immcantation portal* (https://immcantation.readthedocs.io/en/stable/), notably from the change-O toolset[36]. VH and VL sequences, while single cell paired, could only be analyzed independently (VH sequences, then VL sequences), as no method taking this parameter into account currently exists. First, the *AssignGenes.py igblast* tool was run to detect and annotate the V, D, J, CDR and FWR domains in each sequence, using the *IMGT* database (https://www.imgt.org/). Then, *MakeDb.py igblast* converted the result into a readable tsv file. The *ParseDb.py select* tool kept productive sequences, *i.e.*, those for which: (1) the coding region has an open reading frame, (2) no defect are present in the start codon, splicing sites or regulatory elements, (3) no internal stop codons were found, and (4) junction regions are in frame. The clustering of sequences into clonal groups was performed as follows: (1) grouping of the sequences according to same V and J genes (allelic variation not considered) and same length of the CDR3, (2) for each group, computation of the distance score D = (Hamming distance) / (CDR3 length) between each 2 x 2 sequences, (3) determination of the D threshold, that determine whether 2 sequences derive from the same germline cell sequence or not, using the *distToNearest()* function of the *shazam* R package, (4) clone assignment for each sequence, *i.e.*, same ID for sequences belonging to a same clonal group, using the *DefineClones.py* tool. Of note: a few sequences could be lost at that stage, as they did not fit the criteria required by this tool. Then, the putative germline sequence of each clonal group was inferred using the *CreateGermlines.py* tool. Finally, a single *all_passed_seq.tsv* file was obtained for each batch of VH or VL initial fasta files, containing notably, for each sequence, the V, D, J gene and allelic names returned by the *AssignGenes.py igblast* tool, the clone ID, the putative germline sequence before somatic hypermutations, and the

putative V, D, J gene and allelic names of the germline sequence returned by the *CreateGermlines.py* tool.

For phylogenic circos plots (Supp. Fig. 3), productive sequences returned by *ParseDb.py* (see above) were converted into amino-acid sequences. Groups of sequences having the same V and J were extracted from the dataset using Goalign (10.1093/nargab/lqab075) (command goalign subset). Sequences of each group were aligned using ABAlign (10.1093/nar/gkad400) (with options -i <fasta> <-al for light chain or -ah for heavy chain> -sp MU). Phylogenetic trees (Supp. Fig. 3 and Supp. Fig. 6) were then inferred using IQTree v2.2.5 (10.1093/molbev/msaa015) using an antibody-specific model of amino acid substitution (10.1093/molbev/msu340) (options -s <Alignment file> -m AB_model +I+R6 --seed 123456789). Trees, along sequence annotations, were then uploaded to iToL (10.1093/nar/gkae268) using Gotree (10.1093/nargab/lqab075) (command gotree upload itol).

The phylogenetic trees in Supp. Fig. 3 and Supp. Fig. 6 were obtained with the formatClones() and getTrees() functions of the dowser R Package[37], and a homemade function wrapping functions of the ggtree R package[38], for clonal groups with at least 3 non-identical sequences. Amino acid sequence alignments and percentage identity calculations were performed with Jalview software using MUltiple Sequence Comparison by Log- Expectation (Muscle) and colored by percentage identity. Number of mutations were obtained with IMGT database by comparing sequences with germlines and plotted as histograms using GraphPad Prism.

Gene synthesis, cloning and mAbs production

VH and VL synthesis were performed by Synbio Technologies. VHs were cloned into pUC19 vectors containing the sequence encoding the constant regions of human IgG1 heavy-chain (CH), effector-less human IgG1 heavy-chain mutated $N_{297}A$, human IgE heavy-chain. VLs were cloned into pUC19 vectors containing the sequence encoding the constant regions (CL) of human kappa light-chain. Antibodies were produced by transient co-transfection of VH-CH and VL-CL expression plasmids into exponentially growing Freestyle™ HEK 293-F that were cultured in serum-free Freestyle™ 293 Expression Medium (Life Technologies) in suspension at 37°C in a humidified 8% CO_2 incubator on a shaker platform rotating at 110 rpm. Twenty-four hours before transfection, cells were harvested by centrifugation at 300 x g for 5 min and resuspended in expression medium at a density of 1 x 10^6 cells/ml, and cultured overnight in the same conditions

as mentioned above. To produce mAbs, 40 µg of each VH and VL expressing plasmids were diluted in 80 µl of FectoPRO reagent (Polyplus) at a final DNA concentration of 0.8 µg/ml, incubated for 10 minutes at RT before addition to the cells. Twenty-four hours post-transfection, cells were diluted 1:1 with expression medium. Cells were cultured for 6 days after transfection, supernatants were harvested, centrifuged at 1800 g for 40 min and filtered (0.2 µm). Antibodies were purified by affinity chromatography using an AKTA pure FPLC instrument (GE Healthcare) on a HiTrap Protein A Column (GE Healthcare) for human IgG1 and human $IgG1_{N297A}$, and on a anti-human IgE omalizumab-bound affinity column for human IgE, and desalted on a HiTrap Desalting Column (GE Healthcare).

Anti-rocuronium ELISA

96-well plates (Costar) were coated with HSA-rocuronium (mean of 10 rocuronium molecules grafted on a HSA carrier molecule) or HSA at 1 µg/mL in PBS 1X (Gibco) overnight at 4°C overnight, washed 3 times with PBS Tween 20 0.5% (PBST), blocked with PBS-3% BSA, and washed three times with PBST. Mouse serum (diluted 1:250,000-1:5,000-1:100) or monoclonal antibodies were incubated for 2H at room temperature and bound antibodies were detected with HRP-conjugated goat anti-mouse or -human IgG (Bethyl Laboratories) at 1:10,000 dilution. The secondary antibody was revealed using OPD substrate (Sigma-Aldrich) and the reaction stopped with 2M H_2SO_4, and absorbance subsequently recorded at 490 nm and corrected at 620 nm using a spectrophotometer (Biophotometer, Eppendorff). The final OD reported in all graphs/tables corresponds to the subtraction of the OD value of the HSA-rocuronium ELISA minus the OD value of the HSA ELISA. OD values were considered positive if they were at least three times higher than the OD value of the negative control.

Competition ELISA

To ascertain antibody reactivity to rocuronium, and not towards the linker employed to attach rocuronium to HSA, or a neo-epitope formed between rocuronium, the linker and HSA, a competitive inhibition ELISA was developed[7]. This inhibition ELISA also enabled to detect cross-binding of antibodies to a panel of different NMBAs. 96-well plates (Costar) were coated with 1µg/ml HSA-rocuronium at 4°C overnight, washed 3 times with PBST, blocked with PBST containing 3% BSA at room temperature for 2 hours. 300 ng/mL mAbs were pre-incubated with

5-fold serial dilution of free NMBA drug (rocuronium, vecuronium, pancuronium, cisatracurium, atracurium), or NMBA surrogates devoid of quaternary ammoniums (5a-DHT or diisopentyl succinate) from 15,000 µM to 0.96µM.

The antibody-NMBA mixture was added to the ELISA plates and incubated at RT for 2 hours, washed 3 times and revealed with HRP-conjugated goat anti-mouse/human IgG (Bethyl Laboratories) at 1:10,000 dilution. Plates were revealed using an OPD substrate (Sigma-Aldrich). The reaction was stopped with 2M H2SO4 and absorbance was subsequently recorded at 490 nm and corrected at 620 nm using a spectrophotometer (Biophotometer, Eppendorff). For purified mAbs, the IC50 was measured using a non-linear fit [Inhibitor] vs. response -- Variable slope (four parameters) with GraphPad Prism.

Affinity measurements using Bio-Layer Interferometry (BLI)

Affinity of IgG mAbs for rocuronium was tested using Bio-layer interferometry with the OctetRED 384 system. Amine Reactive Second-Generation (AR2G) biosensors were covalently immobilized with HSA-rocuronium mean of 10 rocuronium molecules per HSA carrier molecule), then inserted in wells containing different concentrations of antibodies for 1,800 s (association phase). The antigen-antibody complex was dissociated by introducing the biosensor in the reference buffer (PBS+BSA). Curves were retrieved as raw data from the Octet Data Analysis software and processed in the Scrubber2 software prior to analyses with the Biaevaluation software. IgG-free buffer was used as reference and for background subtraction. Fitting curves and KD values were obtained using the 1:1 Langmuir model.

Affinity measurements using Surface Plasmon Resonance (SPR)

CM5 chips were primed using PBS, washed 3 times with NaOH (50 mM) and SDS (0.1%) 180 seconds each time (5uL/min). At least 5,000 RU of antibody was covalently bound to a CM5 chip by activating using 1:1 NHS:EDC (6,000 s), injecting the antibody (900 s) in acetate buffer pH 5.5 and quenching with EtNH2 (600 s). Free rocuronium was injected (30 µL/min) in PBS-BSA (1 mg/mL) at different concentrations. Signal was subtracted from the signal of the reference canal bound with a non-specific antibody. K_D was determined using a kinetic analysis (RI fixed to 0, model 1:1 binding) with Biaeval software.

Fab preparation

Fab were prepared following Pierce™ Fab Preparation Kit (Thermo scientific) instructions by a 4h digestion with papain in the presence of 4 mM cysteine. After purification on protein A columns, a gel filtration was performed with Tris 50mM pH, 7.4; 100 mM NaCl.

scFv production, purification and characterization

Rocuronium-specific VH and VL sequences were built into scFvs with a polyglycine-serine linker (GGGGS)4 between the VH and VL sequences. The VH-linker-VL sequences were synthesized at Genscript with codon optimization for expression in Drosophila S2 cells, cloned into pT-350 vector using BglII and BstBI restriction sites (the vector is a gift from Dr. Felix Rey, Institut Pasteur, Paris, France). For transfection, $5x10^6$ Drosophila S2 cells were seeded in a T25 conical flask containing 5 ml Schneider's Drosophila medium (Gibco) complemented with 10% fetal bovine serum and incubated at 28°C overnight. Twenty-four hours later, 2 µg of pMT-Roc-scFv-Strep plasmid were co-transfected with 0.1 µg (ratio 20:1) of selection plasmid pCoBlast carrying a gene that confers resistance to puromycin. Effectene transfection kit was used (Qiagen) according to the vendor's protocol. Forty-eight hours after transfection, the selection process was started by addition of puromycin (Invivogen) to the cells at a final concentration of 7 µg/ml. Transfected cells were collected every 4–5 days by centrifugation at 90g for 5 min, and cell pellets were resuspended in fresh medium containing 7 µg/ml puromycin. Cell propagation was initiated ~2 weeks after transfection. Puromycin-selected cells were adapted to serum-free HyClone Insect cell culture media (GE healthcare life science) and were amplified in large volume flasks as needed. Protein expression was induced with 0.5 mM CuSO4 when the cell density reached ~$7.5x10^6$ cells/ml. Seven days after induction, S2 cell suspension was centrifuged for 30 min at 15,000g to remove the cells and the supernatant was collected. Avidin was added at 15 mg/L to sequester any biotin present in the medium. The supernatant, cleared by centrifugation at 20,000g for 30 min and filtration, was loaded onto a Strep-Tactin Superflow high-capacity 5 mL column (IBA GmbH, Göttingen, Germany) using a peristaltic pump or AKTA. The column was washed with 15 mL of 0.1 M Tris pH 8, 0.15 M NaCl, 1 mM EDTA, and the protein was eluted with 8 mL of the same buffer containing 2.5 mM desthiobiotin.

Crystallization and X-ray data collection

Crystallization screening trials were carried out by the vapor diffusion method using a Mosquito TM nanodispensing system (STPLabtech, Melbourn, UK) following established protocols [39]. Briefly, we set up crystallization sitting drops of 400 nL containing a 1:1 mixture of protein sample (Fab or scFv) in complex with 10 mM of rocuronium and crystallization solutions (672 different commercially available conditions) equilibrated against 150 µl of reservoir solution in multiwell plates (Greiner Bio-One). The crystallization plates were stored at 18°C in a RockImager (Formulatrix) automated imaging system to monitor crystal growth. Manual optimization was performed in Linbro plates with the hanging-drop method by mixing 2 µl of protein samples with 2 µl of reservoir solution. The best crystals were obtained with the conditions shown in Supp. Table 1. The crystals were flash cooled in liquid nitrogen for data collection using the crystallization solution as cryoprotectant. . X-ray diffraction data were collected on beamlines PROXIMA-1 and PROXIMA-2A at the synchrotron SOLEIL (St Aubin, France).

Structure determination and model refinement.

The diffraction images for Fab-IP8 and scFv-IP11 were processed with XDS[40], and for Fab-IP2 with autoPROC[41], XDS and STARANISO[42]. Crystallographic calculations were carried out with programs from the CCP4 program suite[43].

The structures of anti-rocuronium Fab and scFv in complex with rocuronium were solved by molecular replacement with Phaser[44] using the structures of the catalytic antibody Fab7A1 (pdb 2AJU) as search model. The final models of the complexes were obtained through interactive cycles of manual model building with Coot[45] and reciprocal-space refinement with Refmac5[46] for the Fab-IP8 and scFv-IP11 complexes, and with Buster[47] for the Fab-IP2 complex. X-ray data collection and model refinement statistics are summarized in Supp. Table 1. Figures showing the crystallographic structures were generated with Pymol (Schrodinger, LLC).

Human mast cell activation test (MAT)

$CD34^+$ precursor cells were isolated from peripheral blood mononuclear cells of healthy donors (provided by the French Blood Bank EFS). $CD34^+$ cells were maintained for 1 week under serum-free conditions using StemSpan medium (9655 Stemcell Technologies) supplemented with recombinant human IL-6 (50 ng/ml; 200-06 Peprotech), human IL-3 (10 ng/ml; 200-03 Peprotech) 3% supernatant of CHO transfectants secreting mouse SCF (a gift from Dr. P. Dubreuil, Marseille,

France, 3% [corresponding to ~50 ng/ml SCF]) and ciprofloxacin (10 ng/mL; 17850-5G-F Sigma Aldrich). Thereafter, the cells were maintained at least 7 weeks in IMDM Glutamax I (31980048), 2-mercaptoethanol (31-350-010), insulin-transferrin selenium (2506865) (all from Gibco), sodium pyruvate (S8636 Sigma Aldrich), 0.5% BSA (A2153 Sigma Aldrich), Penicillin/Streptomycin (100 Units/mL / 100µg/mL; Life Technologies), IL-6 (50 ng/ml 200-06 Peprotech) and 3% supernatant of CHO transfectants secreting mouse SCF. Before their use in experiments, mast cells were tested for phenotype by flow cytometry ($CD117^+$, $Fc\varepsilon RI^+$). Cells were ready for experiments after ~10 weeks in culture (at which time >95% of all cells were $CD117^+$ $Fc\varepsilon RI^+$).

Human mast cells were sensitized overnight with anti-rocuronium human IgE antibodies at 1 µg/mL. Cells were then washed and stimulated with increasing doses of HSA-rocuronium in Tyrode's buffer. Mast cell degranulation was measured by flow cytometry using fluorescent avidin (5 µg/mL; A2170 Invitrogen) which binds to heparin contained in mast cell granules. Data were acquired using a MACSQuant MQ10 flow cytometer (Miltenyi) and analyzed with FlowJo v10.8.1 software (TreeStar).

Hulman basophil activation test (BAT)

Human whole blood was pre-incubated for 3 hours at room temperature with anti-rocuronium IgE at 10 µg/mL. According to manufacturers' instructions (Flow CAST®, FK-CCR, Buhlmann) 50µL of blood was incubated with HSA or HSA-rocuronium for 15 minutes at 37°C with staining reagents (anti-CCR3-PE and anti-CD63 FITC) in an IL-3-containing buffer. Red blood cells were lysed and the cells were analyzed by flow cytometry. Basophils were gated as $SSC^{low}/CCR3^{hi}$ cells and the percentage of $CD63^+$ cells was used as the activation readout.

Neutrophil activation tests

Neutrophils were isolated from fresh human EDTA-drawn blood using the MACSxpress Neutrophil Isolation kit (Miltenyi). Immune complexes were formed for 30 mins at 37°C in HBSS/2%FCS. Flow cytometry: $1x10^5$ neutrophils were stimulated with ICs at a final concentration of 30 µg/mL HSA-Roc and 100 µg/mL anti-Roc IgG in 200µl in HBSS/2% FCS for 30 mins at 37°C, washed and stained with anti-CD62L (clone DREG-56) and anti-CD11b (clone M1/70) (both BD Biosciences) for 15 mins at 4°C, washed and analyzed by flow cytometry on MACSquant16 (Miltenyi). *ROS production*: 5 x 10^4 neutrophils in 100 µl HBSS containing 2%

FCS were incubated with or without stimuli (10 μg/mL HSA-Roc, or indicated pre-formed ICs at a final concentration of 10 μg/mL HSA-Roc and 100 μg/mL anti-Roc IgG) in the presence of 50 μM luminol (Sigma-Aldrich) in a 96-well ViewPlate (Perkin Elmer). Chemiluminescence was measured every 240 seconds using a Spark microplate reader (Tecan) for 2 hours. The area under the curve was calculated for each sample tested in triplicates.

Passive systemic anaphylaxis in mice

hFcεRI^{tg} mFcεRI$^{-/-}$ mice[33] were injected intravenously with 5 μg of anti-rocuronium human IgE mAbs at 0h and challenged 24h later with 2 μg of HSA-roc. Specifically for anti-rocuronium low-affinity mAb IP12, 20 μg of human IgE mAb IP12 was injected intravenously twice at 0h and 24h to favor human IgE biodistribution[48], and mice were challenged 24h later with 100μg of HSA-roc. Control mice were injected with irrelevant human IgE and physiological serum. Central temperature was monitored using a digital thermometer with rectal probe (YSI), and time of death was recorded.

Statistical analyses

The R environment v4.3.1 was used for all the analyses (R foundation, Vienna, Austria. https://www.r-project.org/). Data were neither averaged nor normalized prior to analyses. Response variables were log2 converted when required for better adjustment to linear models. Mixed models using the lmer() function of the lme4 package was used in order to consider the time series (Fig 5B-D), or the random effect of the cell samples (Fig 4B-C) or donors (Fig 4D). In time series (Fig 5B-D), the fixed effect of each treatment was compared to the reference (Physiological Serum) using a t test. Otherwise (Fig 4B-D), effects of treatment were two-by-two compared (contrast comparisons) using the emmeans() function of the emmeans package. Statistical significance was set to a P value of 0.05 or less. In each panel, type I error was controlled by correcting the P values according to the Benjamini & Hochberg method (“BH” option in the p.adjust() function of R).

RESULTS

Anti-rocuronium antibody repertoires in mice are oligoclonal.

To generate the first anti-rocuronium mAbs, we decided to immunize mice against rocuronium and to use rocuronium-specific plasma cells as a source of the highest affinity mAbs[49, 50]. Since rocuronium injections in adjuvant failed to be immunogenic (data not shown), we immunized mice with rocuronium coupled to keyhole limpet hemocyanin (KLH), as a large carrier protein that favors bystander activation. Cervical lymph nodes were collected from two mice displaying the highest anti-rocuronium titer (Fig. 1A), and their cells were encapsulated into microfluidic droplets with fluorescent bioassay reagents and magnetic beads coated with an anti-mouse kappa light chain (Igκ) nanobody (VHH) (Fig. 1B). Immediately after droplet generation, these were subjected to a magnetic field that induced magnetic beads within each droplet to form a line (beadline) (Fig. 1C) and serve as a physical surface for a double-fluorescent sandwich ELISA, revealing IgG secretion from the cell using Alexa Fluor 647-labeled Fc-specific anti-mouse IgG, and specificity of that IgG for rocuronium using Alexa Fluor 488-labeled rocuronium-coupled HSA (Supp. Fig.1, Supp. Fig. 2A). The spatial distribution of fluorescence in the droplets was analyzed by re-injecting them into a second microfluidic chip where each droplet was scanned with superimposed laser lines and epifluorescence was detected using photomultiplier tubes. Secreted IgG and antigen binding were determined from red and green fluorescence localization to the beadline, respectively, and droplets that contained a cell of interest were sorted by fluorescence-activated dielectrophoretic sorting: 3,162 and 3,213 droplets that contained secreted IgG with detectable binding to HSA-rocuronium were sorted from lymph node cells of Mouse1 and Mouse2, respectively (Supp. Fig. 2B). Single cell barcoded-RNA sequencing followed immediately after (Fig. 1D) to retrieve the sequences encoding the variable heavy (VH) and light (VL) chains of the IgG secreted by the sorted plasma cell, as we reported earlier[26]. Sequencing data were processed computationally to identify cell-specific barcodes and to identify cognate VH–VL pairs (one pair per barcode, selecting the most probable VH and VL pair) and were corrected for errors introduced by PCR or sequencing by creation of consensus sequences[26].

Using the *repertoire_profiler* bioinformatic pipeline (refer to the Methods section), we established the anti-rocuronium antibody repertoire profile of the two immunized mice. We

obtained a total of 628 VH and VL pairs from Mouse1 and 421 VH and VL pairs from Mouse2 (Fig. 1E).

Analyses of V(D)J gene usage demonstrated an oligoclonal antibody repertoire profile for both mice. Indeed, for Mouse1, two V_HJ_H and two V_LJ_L rearrangements encoded >91% and >77% of all the VH and VL rearrangements, respectively. Among these, VH1-7_J2/VK2-112_J2 representing 48% and VH1-55_J2/VK4-68_J5 representing 44% of all VH-VL pairs. Strikingly, the latter rearrangement also represented 26% of all VH-VL pairs for Mouse2 (Fig. 1E). Clonal groups were defined as at least three distinct VH-VL pairs with identical VJ gene rearrangement and identical CDR3 length, leading to two VH clonal groups and two VL clonal groups for Mouse1, and 4 VH clonal groups and 15 VL clonal groups for Mouse2. The V1-55_J2 rearrangement represented 33% and 74% of the VH clonal groups, and the V4-68_J5 rearrangement 65% and 51% of the VL clonal groups of Mouse1 and Mouse2, respectively (Fig. 1F). Circos plot representation of the VH-VL pairing highlights these clonal groups among the total repertoire, with a given V_HJ_H rearrangement pairing systematically with a given V_LJ_L rearrangement, with a few exceptions (Fig. 1G). For each VH clonal group, a phylogenic analysis of the VH amino acid sequence was performed, and 15 and 13 VH-VL pairs from the major clonotypes of Mouse1 and Mouse2, respectively, were selected (Supp. Fig. 3A-D) and expressed as chimeric human IgG1,κ for further characterization and validation as anti-rocuronium mAbs.

Anti-rocuronium mAbs interact with rocuronium at high affinity.

Using ELISA, we confirmed that 11 out of 15 (73%) and 7 out of 13 (54%) of mAbs selected from Mouse1 and Mouse2, respectively (Fig. 2A, Table 1) bound HSA-rocuronium. No mAbs among IP6 (V1-75_J3), IP13 (V1-62-2/71_J2), IP14 (V1-85_J2), IP15 (V3-8/3_J3) from Mouse1, and IP28 and IP29 (V3-6_J3), IP30 and IP31 (HV1-18_J2), IP32 (HV1-26_J3) and IP33 (HV1-39_J1) from Mouse2 bound HSA-rocuronium, suggesting that these VH-VL pairs rather bound fluorophores used for cell sorting. To ensure that the other 18 mAbs bound rocuronium and not the linker used to engraft rocuronium onto HSA, we performed competition ELISA in the presence of free NMBA molecules or analogues (Fig. 2B). 9 of these mAbs demonstrated exquisite specificity for rocuronium i.e., IP7, IP8, IP9, IP10, IP12, IP21, IP22 and IP23 (Fig. 2C and Supp. Fig. 4). Indeed, only free rocuronium, but not free molecules with the same aminosteroid scaffold *i.e.*, the closely-related homologues vecuronium and pancuronium, NMBAs atracurium and

cisatracurium, nor 5α-dihydrotestosterone and diisiopentyl succinate that lack quaternary ammonium groups, could inhibit their interaction with HSA-rocuronium. mAbs IP5, IP11, IP24 and IP25 cross-reacted to rocuronium and vecuronium, whereas mAbs IP1, IP2, IP3 and IP4 cross-reacted to rocuronium, vecuronium and pancuronium (Fig. 2C and Supp. Fig. 4). Estimated IC50s of all these cross-reactions indicated 100- to 1,000-fold better affinities for rocuronium than for vecuronium and pancuronium, respectively (Table 1). However, IP26 and IP27 (V3-6_J3) from Mouse2 neither bound free rocuronium not HSA itself, but rather the linker used to couple rocuronium to HSA, or a neoepitope created by this chemical modification. Thus, competitive inhibition ELISA confirmed that only 11 out of 15 (73%) and 5 out of 13 (38%) of mAbs selected initially from Mouse1 and Mouse2, respectively (Table 1), bound free rocuronium.

Identification of these confirmed anti-rocuronium mAbs allowed us to reanalyze the antibody repertoires by only considering the clonal groups those VH or VL rearrangement corresponded to a V_HJ_H or V_LJ_L used in a mAb confirmed to bind free rocuronium. These "functional" repertoires were reduced to 3 VH and 2 VL rearrangements for Mouse1 and a single VH and VL rearrangement for Mouse2 (Supp. Fig. 5A-B), with a mutational load compared to germline showing log-normal-like distributions for Mouse1 and Mouse2 with an average of ~5-7 nucleotide mutations in the VH and ~3-5 in the VL (Supp. Fig. 5C). These functional repertoires highlight unequivocally the absolute pairing of HV1-55_J2 with KV4-68_J5, and of HV1-7_J2 with KV2-112_J2. Even if both mice generated large numbers of HV1-55_J2 encoded sequences that almost exclusively paired to KV4-68_J5, suggestive of a public VH repertoire (identical rearrangements with similar/identical CDR3 size and sequence), CDR sequences diverged largely between the plasma cells from the two mice and clustered separately (Supp. Fig. 6).

As a first exploration of the interaction of these 16 mAbs with rocuronium, we used Bio-layer interferometry (BLI) to measure their avidity towards rocuronium haptenized to HSA with an average molar ratio of 15:1. The avidities of these mAbs were very high towards rocuronium-HSA and ranged from 10 pM to 1.5 nM, except for mAb IP12 at 220 nM (Supp. Fig. 7 and Table 1). The very small size of rocuronium (530 Da) is incompatible with the relatively poor sensitivity of BLI but remains inside the lower limit of detection for Surface Plasmon Resonance (SPR). SPR thus allowed to measure the affinity (K_D) between immobilized mAbs and free rocuronium in solution ranging from 1.2 to 56 nM for all mAbs except mAb IP12 that exhibited a poor K_D of 1.9

mM, in a transitory mode with a very fast association and dissociation (Fig. 2D, Table 1 and Supp. Table 2).

Anti-rocuronium mAbs interact differently with rocuronium.

Rocuronium ring A exists in two different conformations, twist-boat (Fig. 3A) or chair (Fig. 3B)[16], with the sterically less demanding twist-boat conformation being favorable for its accommodation within sugammadex[17]. We thus wondered (i) if anti-rocuronium mAbs would also bind preferentially to one of these conformations, (ii) if the ammonium groups of rocuronium would be essential for the binding as suggested earlier[14, 15], and (iii) if differences in binding modalities existed among the collection of mAbs we identified. We thus performed crystallographic studies with either Fab fragments or single-chain variable fragments (ScFv) of representative mAbs from different clonal groups: IP2 (HV1-55_J2 KV4-68_J5), IP8 (HV1-7_J2_KV2-112_J2) and IP11 (HV1-81_J2 KV2-112_J2) representing the three clonal groups of Mouse1 and the clonal group of Mouse2, and mAbs cross-binding rocuronium and vecuronium (IP2, IP11) and a mAb with exclusive binding to rocuronium (IP8). These antibody fragments and rocuronium co-crystalized efficiently and we solved the structure of Fab-IP2, Fab-IP8, and ScFv-IP11 complexed with rocuronium, respectively, at 2.4 Å, 1.7 Å, and 1.2 Å resolution. (Fig. 3C-E, Supp. Table 1).

In the Fab-IP2 complex, rocuronium interacts with VH and VL like an arrow in a target (Fig. 3C). The allylpyrrolidinium groups encompassing the quaternary ammonium is completely buried in the binding pocket, and the morpholino with the hydroxyl group are exposed to the solvent. This allows vecuronium and pancuronium to bind, as their methylpiperidinium substituent is outside the binding pocket and exposed to the solvent. The precise conformation of the androstane ring A of rocuronium (chair or twist-boat) cannot be precisely determined due to mobility of this region in the structure.

In the co-crystal structure of Fab-IP8 (Fig. 3D), rocuronium is in the twist-boat conformation and interacts differently compared to Fab-IP2 *i.e.*, the Fab-IP8 VH and VL form a pocket inside of which the androstane component of rocuronium binds flat, the hydroxyl group is exposed to the solvent, and the acetoxyl group is buried inside the binding pocket. The specificity for rocuronium and not vecuronium or pancuronium could be explained by the fact that no space remained in the hydrophobic pocket formed by the VH and the VL to accommodate the

methylpiperidinium substituent of vecuronium and pancuronium, and by numerous hydrophobic contacts made by the allyl group of rocuronium.

ScFv-IP11 bound similarly to rocuronium as Fab-IP8, but the binding of rocuronium in its twist-boat conformation induced a rearrangement of the binding site (Fig. 3E). The androstane moiety is stacked between VH residues Trp98 and Tyr56, but unlike IP2 and IP8, the hydroxyl group makes a hydrogen bond with VH Ser54. Interestingly, the stacking interaction with Trp98-H and hydrogen bond with Ser54-H appear to sequester rocuronium in the binding site.

Of note, the hydroxyl group, which served as the attachment point to the rocuronium-carrier proteins used herein for immunization and screening is not involved in the binding, whereas the acetoxyl group is buried inside the binding pocket of all three antibodies. Importantly these co-crystal structures revealed that the allylpyrrolidine substituent containing the quaternary ammonium is completely buried and makes numerous van der Waals contacts with the antibody (Fig. 3C-E), emphasizing the important role of this group in the rocuronium binding mode, in agreement with hypotheses extrapolated from serum cross-reactivity in patients[13, 51]. These data demonstrate that IP2, IP8 and IP11 complexes with rocuronium display an essential role of the quaternary ammonium group for the interaction with antibodies, in a twist-boat or chair conformation, with the hydroxyl group O-atom making a hydrogen bond with Ser54H in the VH of IP11. The ring A twist-boat rocuronium conformation observed in IP8 and IP11 may be due to induced fit, as described for rocuronium-cyclodextrin complexes[17].

Anti-rocuronium mAbs allow to model rocuronium anaphylaxis *in vivo*.

Next, we wondered if anti-rocuronium mAbs expressed as human IgEs could sensitize and promote human mast cell and basophil activation in the presence of rocuronium. Human mast cells and basophils express the high-affinity IgE receptor FcεRI that allows them to be sensitized (pre-armed) with IgE *in vivo* for immediate cell activation following IgE engagement with allergens, leading to rapid anaphylactogenic mediator release. Human mast cells derived from peripheral blood mononuclear cells (PBMC) of healthy donors were used to develop a Mast cell Activation Test (MAT), and whole blood from healthy donors to develop a Basophil Activation Test (BAT) (Fig. 4A). Mast cells sensitized with IP2, IP8 or IP11 human IgEs degranulated in the presence of HSA-rocuronium but not in the presence of free rocuronium or HSA alone. IP12 human IgE weakly degranulated mast cells and only at elevated doses of HSA-rocuronium, as expected from

IP12's poor affinity for rocuronium (Fig. 4B). Similarly, basophils sensitized with IP2, IP8 or IP11, but not IP12, human IgEs became dose-dependently activated in the presence of HSA-rocuronium but not in the presence of free rocuronium (Fig. 4C). Thus, MAT and BAT were positive only in the presence of haptenized, but not free rocuronium, as previously reported[52]. Because we previously reported that NMBA anaphylaxis in humans can engage an IgE pathway but also an IgG pathway leading to neutrophil activation by IgG receptors (FcγR)[9], we investigated neutrophil activation by immune complexes made of anti-rocuronium human IgG mAbs and HSA-rocuronium. Neutrophils from healthy donors expressed elevated levels of CD11b, low levels of CD62L and liberated reactive oxygen species (ROS) when stimulated with immune complexes made of anti-rocuronium human IgG1, but not with immune complexes made of their effector-less variants ($N_{297}A$ mutation of the IgG1 heavy chain), and HSA-rocuronium, when compared to unstimulated controls (Fig. 4D and Supp. Fig. 8).

To test the anaphylactogenic potential of IP2, IP8, IP11 and IP12 human IgEs *in vivo*, we used mice expressing human FcεRI, sensitized them with anti-rocuronium IgEs and challenged them with HSA-rocuronium in a classical model of passive systemic anaphylaxis (Fig. 5A). Rocuronium bound to HSA was used instead of free rocuronium, as the latter induces by itself hypothermia and paralysis. Mice sensitized with increasing doses of IP8 human IgE and subsequently challenged with 2 μg HSA-rocuronium dose-dependently displayed a pronounced drop in central body temperature (Fig. 5B), a hallmark of anaphylaxis in mice[53]. Mice sensitized with 5 μg of IP2, IP8 or IP11 human IgEs, but not unsensitized mice, and challenged with 2 μg HSA-rocuronium displayed a similar drop in central body temperature (Fig. 5C). Thus, although identified from IgG-secreting plasma cells or plasmablasts, the IP2, IP8 and IP11 VH-VL rearrangements generate rocuronium-specific antibodies of high affinity that demonstrate potential as human IgE for human mast cell and basophil activation *in vitro* and induction of anaphylaxis *in vivo* in mice humanized for FcεRI. To induce an IgE-mediated passive systemic anaphylaxis of similar intensity with the lowest affinity anti-rocuronium mAb we identified herein, mAb IP12, it was necessary to increase sensitization 8-fold (40 μg IP12 human IgE) and antigen dose 70-fold (140 μg) (Fig. 5D).

DISCUSSION

In this work, we selected rocuronium, one of the most widely used NMBA, to investigate the rocuronium-specific antibody response in immunized mice and devise the first mouse model of rocuronium anaphylaxis. A cutting-edge high-throughput microfluidic droplet sorting system[26] allowed for the identification of hundreds of rocuronium-specific antibodies from immunized mice. These antibodies were derived from limited V_H-V_L rearrangements and showed convergence between the two immunized mice. The representative antibodies from different rearrangements show high avidity and affinity for rocuronium, and for some examples also crossreactivity to rocuronium chemical family members vecuronium and pancuronium, but not any other NMBA. Co-crystal structures revealed different binding modes of rocuronium by these mAbs, with the ammonium group of rocuronium always involved in the binding. Expressed as human IgE or IgG1 antibodies and aggregated by rocuronium, these antibodies demonstrated *in vitro* efficacy to activate human mast cells and basophils, and human neutrophils, respectively. Passively transferred to mice expressing human IgE receptor FcεRI, high- and low-affinity anti-rocuronium IgE antibodies sensitized mice that developed systemic anaphylaxis upon injection of rocuronium coupled to HSA.

NMBA are small molecules of less than 1 kDa (rocuronium: 530 Da). The antibody repertoire against low molecular weight drugs (<1 kDa) has never been investigated which may be due to the technical difficulty in identifying the scarce drug-specific B cells elicited by poorly or non-immunogenic small compounds. Here we used for B cell screening and sorting plasma cells and plasmablasts from draining lymph nodes that secrete high amounts of IgG, and a bioassay setup and duration that allows accumulation of these IgG onto a physical surface before detection and sorting. Even if we obtained several hundred VH-VL pairs of potential anti-rocuronium mAbs using this approach, we cannot compare it to standard methods for this type of small drug as no other repertoire is currently available. However, by expressing representative VH-VL pairs from the clonal families of these repertoires and considering only those families with confirmed members binding to free rocuronium, we predict that this method allowed to obtain ~700 potential anti-rocuronium mAbs from two immunized mice. The same method applied to large, highly immunogenic, protein antigens demonstrated earlier that from 150 to 530 mAbs could be identified from a single immunized mouse[26].

Bioinformatic analyses of the initial V_H-V_L repertoires identified only two major V_H-V_L rearrangements from both mice, with one (HV1-55_J2/KV4-68_J5) shared between the two mice. Further analyses on representative V_H-V_L pairs expressed as IgG mAbs and extrapolations thereof demonstrated that only these two clonal families (HV1-7_J2 and HV1-55_J2) and the HV1-81_J2 family represented the functional anti-rocuronium repertoire from these immunized mice. These three families represented >90% of the V_H-V_L sequences of Mouse1 but only 25% of the VH-VL sequences of Mouse2. This might be a consequence a largely higher "noise" in the Illumina sequencing of Mouse2 cells compared to Mouse1 cells. In both cases, however, the functional repertoires were oligoclonal and monoclonal, respectively, which might be a consequence of (i) the small size of rocuronium, (ii) the restricted number of mouse germline V_H-V_L sequence able to bind this drug, and/or (iii) the effect of the linker attached to the hydroxyl group of rocuronium that may restrict even more the number of these germline sequences. The mono/oligoclonal nature of the repertoire is not due to the cell population (plasma cells and plasmablasts) chosen or to the droplet microfluidic method used, as we previously reported several highly diverse repertoires of IgG-secreting plasma cells against tetanus toxoid, glucose-6-phosphate isomerase or Tetraspanin-8 covering multiple V-gene families[26]. The mono/oligoclonal nature of the anti-rocuronium repertoires is thus due to the antigen size and nature rather than to the method used to identify these repertoires.

A strong rearrangement convergence was observed between the two mouse repertoires in this study. Convergent (or public) clonotypes (identical rearrangements with similar/identical CDR3 size and sequence) in unrelated individuals with viral infection or vaccination has been reported in particular for IGK and IGL due to the lack of combination diversity and junction diversity during light chain rearrangement[54, 55], but less so for IGH[56, 57]. These public VLs were able to pair with diverse VHs in multiple donors[58]. In our work, two V_LJ_L rearrangements (KV2-112_J2 and KV4-68_J5) paired with over 90% of VH sequences in the two mice analyzed. Within the functional repertoire we identified herein, HV1-55_J2 paired exclusively with KV4-68_J5 and HV1-7_J2 exclusively with KV2-112_J2, suggesting that these pairings are required for rocuronium binding. Indeed, exchanging light chains between HV1-55_J2 and HV1-7_J2 mAbs (i.e., between IP2 and IP8, or between IP5 and IP7), led to a loss of binding to rocuronium (data not shown). For the HV1-81_J2 clonal group, we expressed two mAbs that shared the same VH rearrangement with identical CDRH1 and CDRH3, and only 2 amino acid mutations in the

CDRH2, one mAb with light chain KV2-112_J2 (IP11) and one mAb with light chain KV4-68_J5 (IP12): these demonstrated a ~35,000-fold difference in affinity for rocuronium in favor of IP11. Due to the barcoding method used (split-and-pool synthesis) in the single cell sequencing method and the probabilistic pairing of the most abundant V_H and V_L associated to a given barcode, we wondered if IP12 was not the consequence of a V_H-V_L mispairing that led to the recombinant expression of this antibody, whereas it should have been paired with a more "favorable" light chain for this heavy chain rearrangement i.e., KV2-112_J2. Indeed, when we expressed the VH of IP11 with the V_L of IP12, the avidity for HSA-rocuronium was equivalent to that of IP12 and when we expressed the V_H of IP12 with the V_L of IP11 the avidity was equivalent to that of IP11 (data not shown). The less common V_L pairings to V_H found in these repertoires may therefore mostly/all result in lower affinity antibodies or loss of binding, and one could propose to choose in the probability ranking the first "favorable V_L i.e., a KV4-68_J5 VL systematically for a V1-55_J2 and a KV2-112_J2 V_L systematically for a V1-7_J2 V_H or a V1-81_J2 V_H. This method may result in ameliorating affinity for rocuronium but would reduce the diversity in these repertoires by excluding rare VH-VL pairings.

The ability of the anti-rocuronium mAbs we identified herein either to bind specifically rocuronium or to cross-bind vecuronium and pancuronium was explained by the three co-crystal structures of antibody fragments of IP2, IP8 and IP11 in complex with rocuronium that we reported herein. These three different structures represent the binding mode of one representative of each VH family V1-55_J2, V1-7_J2 and V1-81_J2 and all reveal that both VH and VL of each mAb are involved in the binding, and that the allylpyrrolidinium substituent containing the quaternary ammonium of rocuronium is completely buried in the binding cleft of the antibodies. These co-crystal structures of mAbs with rocuronium, even if these mAbs were raised in mice immunized with rocuronium haptenized onto a carrier protein, are thus in agreement with hypotheses extrapolated from serum cross-reactivity in patients suggesting that the ammonium group is part of the binding interaction with antibodies[13, 51]. In the same manner as in rocuronium-sugammadex complexes, rocuronium bound IP2, IP8 and IP11 in a twist-boat or chair conformation which might be due to induced fit, as reported for rocuronium-sugammadex complexes[17] or by the selection among the two rocuronium conformers. Crossreactivity with vecuronium and pancuronium required that their different substituents (compared to rocuronium) would remain outside the binding pocket and be exposed to the solvent. Cross-binding had already been reported decades

ago for IgE antibodies in the serum of patients with NMBA hypersensitivity to alcuronium: their binding to alcuronium was inhibited strongly by tubocurarine, modestly by pancuronium and weakly by decamethonium and gallamine, and even less by succinylcholine[18]. If these types of cross-binding represent the property of a single mAb in each patient sera or that of different populations of antibodies within each serum that each recognize a different NMBA with little or no cross-reactivity with other NMBA remains unknown. Surprisingly however, the three co-crystal structures we report herein highlighted three different binding modalities for such a small antigen and such restricted repertoire with only 3 VHs and 2 VLs, with mAbs IP8 and IP11 using the same VL rearrangement KV2-112_J2 but binding to rocuronium with different modalities. Whether our results are predictive of antibodies involved in NMBA hypersensitivity in humans remains to be clarified and human anti-rocuronium antibody repertoires to be explored.

This first description of anti-rocuronium mAbs isolated from plasma cells and plasmablasts allowed us to demonstrate their ability to induce cell activation when aggregated by rocuronium. As we reported earlier for NMBA hypersensitivity in humans, at least two activation pathways co-exist that lead to severe anaphylactic reaction to NMBAs, the IgE pathway leading to mast cell and basophil activation and the IgG pathway leading to neutrophil and platelet activation[59]. All the high-affinity anti-rocuronium mAbs expressed as human IgEs activated *in vitro* human mast cells and basophils, and expressed as human IgG1s activated human neutrophils, in the presence of haptenized rocuronium, but not free rocuronium. A previous study using IgE-stripped human basophils sensitized with patient serum containing polyclonal anti-rocuronium IgE also reported that only haptenized rocuronium but not free rocuronium induced basophil activation *in vitro*[52]. From the co-crystals of these mAbs with rocuronium, it appears unlikely that a single rocuronium molecule could be bound by two different mAbs; rocuronium being engulfed in the antibody binding site of a single antibody, providing no epitope for a second antibody to bind. A molecular partner may thus exist that allows rocuronium haptenization to induce cell activation and anaphylaxis in humans. Alternatively, patients may produce particular antibodies that could bind at least in pairs to a single rocuronium molecule to induce FcεRI aggregation and cell activation, but our recent study on anti-)rocuronium mAbs from human memory B cells do not favor this latter hypothesis[7]. Importantly, once passively transferred into mice expressing human IgE receptors, both high- and low-affinity anti-rocuronium IgE mAbs led to severe anaphylactic reactions *in vivo* upon exposure to haptenized rocuronium. Rocuronium is indeed devoid of

neuromuscular blocking properties once haptenized onto a larger protein that cannot freely diffuse into the neuromuscular junction. This strategy allowed us to generate for the first time a model of rocuronium-induced anaphylaxis in mice and to follow anaphylaxis by central body temperature. More complex setups including anesthesia, intubation and artificial ventilation could be envisioned to model anaphylaxis with free rocuronium, but these would require using other parameters than body temperature or cardiac rhythm- that are uncontrolled during anesthesia - to monitor anaphylaxis, and potentially larger animals like non-human primates to increase the relevance to human physiopathology.

This work could not have been performed without chemically modifying rocuronium which represents a limitation of this study. We used rocuronium derivatives by extending the OH group with a functionalized linker for grafting on carrier proteins KLH and HSA that were used for B cell sorting, ELISA, avidity measurements, and functional assays. This strategy allowed for identification of anti-rocuronium antibodies with no crossreactivity for NMBAs from other families outside aminosteroids, not even to dihydrotestosterone, a rocuronium mimetic devoid of ammonium groups. Validated by other groups, these anti-rocuronium IgE or IgG mAbs could be used as internal standards and references in routine assays like skin prick tests, basophil activation tests, or the more recently developed mast cell activation tests[60]. Another limitations is the use of rocuronium to immunize mice, whereas patients become sensitized in the vast majority without any exposure to rocuronium but to other ammonium-containing compounds present in cough syrup, cosmetics, hair dyes, household cleaning products or drugs at the probable initiation of the immune reaction towards rocuronium[7, 61].

In conclusion, this work reports on the underlying mechanisms of anaphylactic reactions to NMBAs by identifying the first anti-rocuronium antibody repertoires from immunized mice, suggests novel diagnostic tools for rocuronium hypersensitivity, and provides a proof-of-concept for modeling NMBA hypersensitivity *in vivo* in mice.

REFERENCES

1. Thilen SR, Weigel WA, Todd MM, Dutton RP, Lien CA, Grant SA, et al. 2023 American Society of Anesthesiologists Practice Guidelines for Monitoring and Antagonism of Neuromuscular Blockade: A Report by the American Society of Anesthesiologists Task Force on Neuromuscular Blockade. Anesthesiology 2023; 138:13-41.
2. Fuchs-Buder T, Romero CS, Lewald H, Lamperti M, Afshari A, Hristovska AM, et al. Peri-operative management of neuromuscular blockade: A guideline from the European Society of Anaesthesiology and Intensive Care. Eur J Anaesthesiol 2023; 40:82-94.
3. Lien CA, Eikermann M. Neuromuscular Blockers and Reversal Drugs. Pharmacology and Physiology for Anesthesia (Second Edition) 2019:428-54.
4. Mertes PM, Aimone-Gastin I, Gueant-Rodriguez RM, Mouton-Faivre C, Audibert G, O'Brien J, et al. Hypersensitivity reactions to neuromuscular blocking agents. Curr Pharm Des 2008; 14:2809-25.
5. Sadleir PH, Clarke RC, Bunning DL, Platt PR. Anaphylaxis to neuromuscular blocking drugs: incidence and cross-reactivity in Western Australia from 2002 to 2011. Br J Anaesth 2013; 110:981-7.
6. Mertes PM, Ebo DG, Garcez T, Rose M, Sabato V, Takazawa T, et al. Comparative epidemiology of suspected perioperative hypersensitivity reactions. Br J Anaesth 2019; 123:e16-e28.
7. Dejoux A, Zhu Q, Ganneau C, Goff OR, Godon O, Lemaitre J, et al. Rocuronium-specific antibodies drive perioperative anaphylaxis but can also function as reversal agents in preclinical models. Sci Transl Med 2024; 16:eado4463.
8. Bruhns P, Chollet-Martin S. Mechanisms of human drug-induced anaphylaxis. J Allergy Clin Immunol 2021; 147:1133-42.
9. Jonsson F, de Chaisemartin L, Granger V, Gouel-Cheron A, Gillis CM, Zhu Q, et al. An IgG-induced neutrophil activation pathway contributes to human drug-induced anaphylaxis. Sci Transl Med 2019; 11.
10. Winbery SL, Lieberman PL. Histamine and antihistamines in anaphylaxis. Clin Allergy Immunol 2002; 17:287-317.
11. Conte B, Zoric L, Bonada G, Debaene B, Ripart J. Reversal of a rocuronium-induced grade IV anaphylaxis via early injection of a large dose of sugammadex. Can J Anaesth 2014; 61:558-62.
12. Kim SM, Oh SH, Ryu SA. Treatment of rocuronium-induced anaphylaxis using sugammadex - A case report. Anesth Pain Med (Seoul) 2021; 16:56-9.
13. Baldo BA, Fisher MM. Substituted ammonium ions as allergenic determinants in drug allergy. Nature 1983; 306:262-4.
14. Russell WJ, Lee C, Milne D. Is allergy to rocuronium a high probability cross-reaction with suxamethonium? Anaesth Intensive Care 2003; 31:333.
15. Rose MA, Anderson J, Green SL, Yun J, Fernando SL. Morphine and pholcodine-specific IgE have limited utility in the diagnosis of anaphylaxis to benzylisoquinolines. Acta Anaesthesiol Scand 2018; 62:628-34.
16. Fielding L, Grant GH. Conformational equilibria in amino steroids. 1. A proton and carbon-13 NMR spectroscopy and molecular mechanics study of 3.alpha.-hydroxy-2.beta.-(4-morpholinyl)-5.alpha.H-androstan-17-one. J. Am. Chem. Soc. 1991; 113:9785-90.
17. Cooper A, Nutley M, MacLean EJ, Cameron K, Fielding L, Mestres J, et al. Mutual induced fit in cyclodextrin-rocuronium complexes. Org Biomol Chem 2005; 3:1863-71.
18. Baldo BA, Fisher MM, Pham NH. On the origin and specificity of antibodies to neuromuscular blocking (muscle relaxant) drugs: an immunochemical perspective. Clin Exp Allergy 2009; 39:325-44.
19. Peyneau M, de Chaisemartin L, Gigant N, Chollet-Martin S, Kerdine-Romer S. Quaternary ammonium compounds in hypersensitivity reactions. Front Toxicol 2022; 4:973680.
20. Florvaag E, Johansson SG. The Pholcodine Case. Cough Medicines, IgE-Sensitization, and Anaphylaxis: A Devious Connection. World Allergy Organ J 2012; 5:73-8.
21. Mertes PM, Petitpain N, Tacquard C, Delpuech M, Baumann C, Malinovsky JM, et al. Pholcodine exposure increases the risk of perioperative anaphylaxis to neuromuscular blocking agents: the ALPHO case-control study. Br J Anaesth 2023.
22. van der Poorten MM, Van Gasse AL, Hagendorens MM, Faber MA, De Puysseleyr L, Elst J, et al. Serum specific IgE antibodies in immediate drug hypersensitivity. Clin Chim Acta 2020; 504:119-24.
23. Decuyper, II, Ebo DG, Uyttebroek AP, Hagendorens MM, Faber MA, Bridts CH, et al. Quantification of specific IgE antibodies in immediate drug hypersensitivity: More shortcomings than potentials? Clin Chim Acta 2016; 460:184-9.

24. Wardemann H, Busse CE. Novel Approaches to Analyze Immunoglobulin Repertoires. Trends Immunol 2017; 38:471-82.
25. Victora GD, Nussenzweig MC. Germinal Centers. Annu Rev Immunol 2022; 40:413-42.
26. Gerard A, Woolfe A, Mottet G, Reichen M, Castrillon C, Menrath V, et al. High-throughput single-cell activity-based screening and sequencing of antibodies using droplet microfluidics. Nat Biotechnol 2020; 38:715-21.
27. Lindeman I, Zhou C, Eggesbo LM, Miao Z, Polak J, Lundin KEA, et al. Longevity, clonal relationship, and transcriptional program of celiac disease-specific plasma cells. J Exp Med 2021; 218.
28. Canales-Herrerias P, Crickx E, Broketa M, Sokal A, Chenon G, Azzaoui I, et al. High-affinity autoreactive plasma cells disseminate through multiple organs in patients with immune thrombocytopenic purpura. J Clin Invest 2022; 132.
29. Ehling RA, Weber CR, Mason DM, Friedensohn S, Wagner B, Bieberich F, et al. SARS-CoV-2 reactive and neutralizing antibodies discovered by single-cell sequencing of plasma cells and mammalian display. Cell Rep 2022; 38:110242.
30. Reddy JI, Cooke PJ, van Schalkwyk JM, Hannam JA, Fitzharris P, Mitchell SJ. Anaphylaxis is more common with rocuronium and succinylcholine than with atracurium. Anesthesiology 2015; 122:39-45.
31. Takazawa T, Mitsuhata H, Mertes PM. Sugammadex and rocuronium-induced anaphylaxis. J Anesth 2016; 30:290-7.
32. Tacquard C, Collange O, Gomis P, Malinovsky JM, Petitpain N, Demoly P, et al. Anaesthetic hypersensitivity reactions in France between 2011 and 2012: the 10th GERAP epidemiologic survey. Acta Anaesthesiol Scand 2017; 61:290-9.
33. Mancardi DA, Iannascoli B, Hoos S, England P, Daeron M, Bruhns P. FcgammaRIV is a mouse IgE receptor that resembles macrophage FcepsilonRI in humans and promotes IgE-induced lung inflammation. J Clin Invest 2008; 118:3738-50.
34. Eyer K, Doineau RCL, Castrillon CE, Briseno-Roa L, Menrath V, Mottet G, et al. Single-cell deep phenotyping of IgG-secreting cells for high-resolution immune monitoring. Nat Biotechnol 2017; 35:977-82.
35. Djaffardjy M, Marchment G, Sebe C, Blanchet R, Bellajhame K, Gaignard A, et al. Developing and reusing bioinformatics data analysis pipelines using scientific workflow systems. Comput Struct Biotechnol J 2023; 21:2075-85.
36. Gupta NT, Vander Heiden JA, Uduman M, Gadala-Maria D, Yaari G, Kleinstein SH. Change-O: a toolkit for analyzing large-scale B cell immunoglobulin repertoire sequencing data. Bioinformatics 2015; 31:3356-8.
37. Hoehn KB, Pybus OG, Kleinstein SH. Phylogenetic analysis of migration, differentiation, and class switching in B cells. PLoS Comput Biol 2022; 18:e1009885.
38. Yu G. Using ggtree to Visualize Data on Tree-Like Structures. Curr Protoc Bioinformatics 2020; 69:e96.
39. Weber P, Pissis C, Navaza R, Mechaly AE, Saul F, Alzari PM, et al. High-Throughput Crystallization Pipeline at the Crystallography Core Facility of the Institut Pasteur. Molecules 2019; 24.
40. Kabsch W. Xds. Acta Crystallogr D Biol Crystallogr 2010; 66:125-32.
41. Vonrhein C, Flensburg C, Keller P, Sharff A, Smart O, Paciorek W, et al. Data processing and analysis with the autoPROC toolbox. Acta Crystallogr D Biol Crystallogr 2011; 67:293-302.
42. Tickle IJ, Flensburg, C., Keller, P., Paciorek, W., Sharff, A., Vonrhein, C., Bricogne, G. STARANISO (http://staraniso.globalphasing.org/cgi-bin/staraniso.cgi). Cambridge, United Kingdom: Global Phasing Ltd. 2016.
43. Agirre J, Atanasova M, Bagdonas H, Ballard CB, Basle A, Beilsten-Edmands J, et al. The CCP4 suite: integrative software for macromolecular crystallography. Acta Crystallogr D Struct Biol 2023; 79:449-61.
44. McCoy AJ, Grosse-Kunstleve RW, Adams PD, Winn MD, Storoni LC, Read RJ. Phaser crystallographic software. J Appl Crystallogr 2007; 40:658-74.
45. Emsley P, Cowtan K. Coot: model-building tools for molecular graphics. Acta Crystallogr D Biol Crystallogr 2004; 60:2126-32.
46. Murshudov GN, Skubak P, Lebedev AA, Pannu NS, Steiner RA, Nicholls RA, et al. REFMAC5 for the refinement of macromolecular crystal structures. Acta Crystallogr D Biol Crystallogr 2011; 67:355-67.
47. Bricogne G, Blanc E, Brandl M, Flensburg C, Keller P, Paciorek W, et al. BUSTER version X.Y.Z. Cambridge, United Kingdom: Global Phasing Ltd. 2017.
48. Dombrowicz D, Brini AT, Flamand V, Hicks E, Snouwaert JN, Kinet JP, et al. Anaphylaxis mediated through a humanized high affinity IgE receptor. J Immunol 1996; 157:1645-51.

49. Ise W, Kurosaki T. Plasma cell differentiation during the germinal center reaction. Immunol Rev 2019; 288:64-74.
50. Suan D, Sundling C, Brink R. Plasma cell and memory B cell differentiation from the germinal center. Curr Opin Immunol 2017; 45:97-102.
51. Baldo BA, Fisher MM. Anaphylaxis to muscle relaxant drugs: cross-reactivity and molecular basis of binding of IgE antibodies detected by radioimmunoassay. Mol Immunol 1983; 20:1393-400.
52. Aalberse RC, Kleine Budde I, Mulder M, Stapel SO, Paulij W, Leynadier F, et al. Differentiating the cellular and humoral components of neuromuscular blocking agent-induced anaphylactic reactions in patients undergoing anaesthesia. Br J Anaesth 2011; 106:665-74.
53. Gouel-Cheron A, Dejoux A, Lamanna E, Bruhns P. Animal Models of IgE Anaphylaxis. Biology (Basel) 2023; 12.
54. Hoi KH, Ippolito GC. Intrinsic bias and public rearrangements in the human immunoglobulin Vlambda light chain repertoire. Genes Immun 2013; 14:271-6.
55. Jackson KJ, Wang Y, Gaeta BA, Pomat W, Siba P, Rimmer J, et al. Divergent human populations show extensive shared IGK rearrangements in peripheral blood B cells. Immunogenetics 2012; 64:3-14.
56. Parameswaran P, Liu Y, Roskin KM, Jackson KK, Dixit VP, Lee JY, et al. Convergent antibody signatures in human dengue. Cell Host Microbe 2013; 13:691-700.
57. Jackson KJ, Liu Y, Roskin KM, Glanville J, Hoh RA, Seo K, et al. Human responses to influenza vaccination show seroconversion signatures and convergent antibody rearrangements. Cell Host Microbe 2014; 16:105-14.
58. DeKosky BJ, Kojima T, Rodin A, Charab W, Ippolito GC, Ellington AD, et al. In-depth determination and analysis of the human paired heavy- and light-chain antibody repertoire. Nat Med 2015; 21:86-91.
59. Beutier H, Hechler B, Godon O, Wang Y, Gillis CM, de Chaisemartin L, et al. Platelets expressing IgG receptor FcgammaRIIA/CD32A determine the severity of experimental anaphylaxis. Sci Immunol 2018; 3.
60. Elst J, Van Houdt M, van der Poorten MM, Van Gasse AL, Mertens C, Toscano A, et al. Comparison of the passive mast cell activation test with the basophil activation test for diagnosis of perioperative rocuronium hypersensitivity. Br J Anaesth 2023.
61. Orihara M, Takazawa T, Horiuchi T, Sakamoto S, Nagumo K, Tomita Y, et al. Comparison of incidence of anaphylaxis between sugammadex and neostigmine: a retrospective multicentre observational study. Br J Anaesth 2020; 124:154-63.

ACKNOWLEDGMENTS

We would like to thank our colleagues from the Institut Pasteur, Paris, France for their help and advice: Delphine Brun and Annalisa Meola (Structural virology unit) for ScFv generation and production; Bertrand Raynal, Sébastien Brulé and Sylviane Hoos for assistance with affinity measurements (Molecular Biophysics Core Facility), Fabrice Agou for access to the BLI instrument (Plateforme de Criblage Chémogénomique et Biologique; PF-CCB), Michel Perez for advice and support (Direction Des Applications De la Recherche et des Relations Industrielles; DARRI), Odile Richard-Le Goff for training and Henna Maulaboksh for administrative help. We would like to thank the staff of the crystallography platform at Institut Pasteur for crystallization screening, and acknowledge synchroton SOLEIL (Saint-Aubin, France) for granting access to their facility and the staff of Proxima1 and Proxima2A for helpful assistance. The mast cell activation tests performed using flow cytometry were done at the INFINITy INSERM UMR1291 core facility connected to Toulouse Réseau Imagerie network, member of the France BioImaging national infrastructure supported by the French National Research Agency (ANR 10 INBS 04).

No AI-based solution has been used to write this manuscript.

FUNDING

Work in the Bruhns' lab was supported by the Institut Pasteur, Institut National de la Santé et de la Recherche Médicale (Inserm), Fondation pour la Recherche Médicale, Paris, France (Programme Equipe FRM grant EQU202203014631 to PB), Accélérateur de l'innovation de l'Institut Pasteur (grant rocuCEPT to PB), Agence Nationale de la Recherche (grants ANR-14-CE16-0011 « DROPmAbs », ANR-16-CARN-0023-01 and ANR-21-CE15-0027 « CURAREP » to PB), European Research Council (ERC)–Seventh Framework Program (ERC-2013-CoG 616050 to PB) and Inserm *International Research Program* (IRP grant ALLERGYMINE to PB). AD was supported by a doctoral fellowship from Sorbonne Université, followed by a fellowship from the Fondation pour la Recherche Médicale (grant FDT202304016860 to AD). QZ received a PhD scholarship from the Chinese Science Council. AGC was a recipient of a poste d'accueil 2017 Institut Pasteur – Assistance Publique des Hôpitaux de Paris (APHP), and was supported by a grant provided by INSERM, SFAR (Société Française d'Anesthésie et de Réanimation), and SRLF (Société de Réanimation de Langue Française) through the "Bourse de Recherche du Comité

d'interface INSERM-SFAR-SRLF 2012 to AGC. CMG was supported partly by a stipend from the Pasteur-Paris University (PPU) International PhD program and by the Institut Carnot Pasteur Maladies Infectieuses. CC acknowledges financial support from CONCYTEC, Peru. PB benefited from an additional support from AP-HP through a "Contrat Local d'Interface 2014" and the "Département Hospitalo-Universitaire" (DHU) FIRE.

AUTHOR CONTRIBUTIONS

Experimental design: SB, AG, FJ, SCM and PB; Conducting experiments: AD, QZ, OG, SE, GM, CG, CC, CP, CG, BI, LdC, AH, FJ. Data analyses and discussions: AD, QZ, AW, OG, GM, CG, FL, FS, PE, LLR, AGC, LdC, AH, GAM, SB, AG, FJ, SCM and PB. Funding acquisition: PB; Writing (original draft): AD and PB; Writing (review and editing): all authors.

COMPETING INTERESTS

Unrelated to the submitted work, PB received consulting fees from Regeneron Pharmaceuticals. LdC (Luc de Chaisemartin) reports lecture fees from MSD France, without any relation to the content of this manuscript. L.L.R has received grants and/or consulting fees from Neovacs, CEVA, Novartis and Argenx, not related to this work. A.G. is a co-founder and employee of Saber Bio SAS and former HiFiBiO Therapeutics SAS employee. Patents have been filed on some aspects of this work and future development of the platform, and the inventors may receive payments related to exploitation of these under their employer's rewards to inventors scheme. The other authors declare no competing interests.

DATA AND MATERIALS AVAILABILITY

Coordinates and structure factors of Fab-IP2, Fab-IP8, and scFv-IP11 have been deposited in the Protein Data Bank with accession codes 9G6S, 9G6R, and 9G6Q, respectively.

Further information and requests for resources, reagents and material should be directed to and will be fulfilled by the Lead Contact, Pierre Bruhns bruhns@pasteur.fr

TABLES

Table 1: Characteristics of mAbs expressed from repertoires of Mouse1 and Mouse2. Indicated mAbs were measured for binding to HSA-rocuronium by BLI (avidity), to free rocuronium by SPR (affinity), and evaluated for cross-reactivity to rocuronium (R), vecuronium (V) and pancuronium (P) by competition in the HSA-rocuronium ELISA (specificity and IC50 values). Number of amino acid (aa) mutations differences (≠) compared to the germline sequence are indicated for the heavy chain variable region (VH) and the light chain variable region (VL). NB, not binding; nt, not tested; IC50, Half-maximal inhibitory concentration. Identical colors indicate identical gene families used in V-J rearrangements.

		Sanger sequencing				BLI	SPR	Competition ELISA				Mutations	
	mAb	VH gene	JH gene	VL gene	JL gene	Avidity for HSA-roc (nM)	Affinity for free roc (nM)	Specificity	IC50 Roc (µM)	IC50 Vec (µM)	IC50 Panc (µM)	VH aa ≠	VL aa ≠
Mouse1	**IP1**	V1-55	J2	KV4-68	KJ5	**0.9**	nt	R-V-P	**0.3**	**177**	**6,995**	3	5
	IP2	V1-55	J2	KV4-68	KJ5	**0.6**	**3.9**	R-V-P	**3.8**	**20**	**787**	3	4
	IP3	V1-55	J2	KV4-68	KJ5	**1.2**	nt	R-V-P	**1.3**	**110**	**737**	3	4
	IP4	V1-55	J2	KV4-68	KJ5	**0.9**	nt	R-V-P	**3.1**	**240**	**3,635**	7	3
	IP5	V1-55	J2	KV4-68	KJ5	**0.4**	nt	R-V	**289**	**615**	-	6	3
	IP6	*V1-75*	*J3*	*KV6-25*	*KJ1*	*NB*	*nt*	*nt*	*nt*	*nt*	*nt*	*6*	*7*
	IP7	V1-7	J2	KV2-112	KJ2	**0.82**	nt	R	**4.4**	-	-	9	3
	IP8	V1-7	J2	KV2-112	KJ2	**0.46**	**1.0**	R	**3.3**	-	-	3	3
	IP9	V1-7	J2	KV2-112	KJ2	**0.8**	nt	R	**3.5**	-	-	4	2
	IP10	V1-7	J2	KV2-112	KJ2	**0.86**	nt	R	**5.0**	-	-	8	5
	IP11	V1-81	J2	KV2-112	KJ2	**0.53**	**56**	R-V	**5.0**	**548**	-	5	1
	IP12	V1-81	J2	KV4-68	KJ5	**220**	**1,990,000**	R	**2,572**	-	-	4	4
	IP13	*V1-62-2/71*	*J2*	*KV19-93*	*KJ2*	*NB*	*nt*	*nt*	*nt*	*nt*	*nt*	*5*	*7*
	IP14	*V1-85*	*J2*	*KV6-13*	*KJ2*	*NB*	*nt*	*nt*	*nt*	*nt*	*nt*	*9*	*7*
	IP15	*V3-8/3*	*J1*	*KV14-111*	*KJ1*	*NB*	*nt*	*nt*	*nt*	*nt*	*nt*	*5*	*8*
Mouse2	**IP21**	V1-55	J2	KV4-68	KJ5	**0.13**	nt	R	**26**	-	-	10	6
	IP22	V1-55	J2	KV4-68	KJ5	**0.2**	nt	R	**14**	-	-	6	1
	IP23	V1-55	J2	KV4-68	KJ5	nt	nt	R	**109**	-	-	9	8
	IP24	V1-55	J2	KV4-68	KJ5	**0.01**	**12**	R-V	**18**	nt	-	6	1
	IP25	V1-55	J2	KV4-68	KJ5	nt	nt	R-V	**20**	**682**	-	2	1
	IP26	*V3-6*	*J3*	*KV12-89*	*GKJ4*	*Binding linker or neoepitope*						*3*	*0*
	IP27	*V3-6*	*J3*	*KV12-89*	*GKJ4*	*Binding linker or neoepitope*						*7*	*1*
	IP28	*V3-6*	*J3*	*KV10-94*	*KJ2*	*NB*	*nt*	*nt*	*nt*	*nt*	*nt*	*3*	*4*
	IP29	*V3-6*	*J3*	*KV10-94*	*KJ2*	*NB*	*nt*	*nt*	*nt*	*nt*	*nt*	*6*	*4*
	IP30	*HV1-18*	*J2*	*KV6-17*	*KJ5*	*NB*	*nt*	*nt*	*nt*	*nt*	*nt*	*1*	*7*
	IP31	*HV1-18*	*J2*	*KV6-17*	*KJ5*	*NB*	*nt*	*nt*	*nt*	*nt*	*nt*	*4*	*10*
	IP32	*HV1-26*	*J3*	*KV12-46*	*J2*	*NB*	*nt*	*nt*	*nt*	*nt*	*nt*	*12*	*4*
	IP33	*HV1-39*	*J1*	*KV12-44*	*KJ2*	*NB*	*nt*	*nt*	*nt*	*nt*	*nt*	*5*	*3*

FIGURE LEGENDS

Figure 1. Generation of rocuronium-specific antibody repertoires from immunized mice. (**A**) Schematic of mice immunization strategy and blood sampling (top) and IgG anti-rocuronium ELISA results from sera of mice immunized with KLH-rocuronium or KLH (bottom). (**B-D**) Schematic representation of droplet microfluidic steps: (**C**) droplet generation, (**C**) droplet sorting, (**D**) in-droplet single cell reverse transcription and barcoding. PMTs, photomultipliers. (**E-F**) Donut plots of the VJ gene usage among (E) all the VH (left) and VL (right) or among (F) the clonal groups (identical VJ genes and CDR3 length) identified from Mouse1 (top) and Mouse2 (bottom). The central value indicates the number of sequences. VH-VL pairs corresponding to mAbs further characterized in this work are indicated (IP1-IP12 for Mouse1 and IP21-IP33 for Mouse2). The 5 most representative VJ families are colored and labeled, the others are in shades of grey. (**G**) Circos plots of the pairing of VH clonal groups from (F) with their VL rearrangement for Mouse1 (left) and Mouse2 (right).

Figure 2: Characterization of rocuronium-specific mAbs from immunized mice. (**A**) Rocuronium-specific ELISA of representative IgG mAbs from indicated mice. (**B**) Structural formula of indicated molecules. (**C**) Competition ELISA of anti-rocuronium IgG ELISA at fixed concentration of mAbs but increasing concentrations of indicated molecules free in solution. 5a-DHT, 5-alpha-dihydrotestosterone; DS, diisiopentyl succinate; QA, quaternary ammonium. (**D**) Left, scheme of surface plasmon resonance (SPR) affinity measurements. Right, SPR results for the interaction between immobilized mAbs and varying concentrations of free rocuronium in solution. The K_D was obtained by fitting the curves using a heterogenous ligand model. RU, resonance unit.

Figure 3: Crystal structures of mAbs in complex with rocuronium. (A) Rocuronium twist-boat conformation. (**B**) Rocuronium chair conformation. **(C-E)** Top: surface representation of co-crystal structures of rocuronium-specific (**C**) Fab-IP2, (**D**) Fab-IP8 and (**E**) scFv-IP11. Bottom: superposition of the rocuronium and key residues of the binding site. The rocuronium molecule is

shown in yellow and the antibody heavy chain and light chain are colored in green and cyan, respectively. O atoms are in red, N atoms in blue.

Figure 4: Anti-rocuronium mAbs activate human mast cells, basophils and neutrophils following aggregation by rocuronium. (**A**) Schematic representation of activation tests. (**B**) Human mast cell and (**C**) human basophil activation test using hIgE for sensitization, followed by challenge with free rocuronium (Free roc), HSA or HSA-rocuronium, with degranulation measured using fluorescent avidin or anti-CD63 staining, respectively. Mean ± standard deviation of results from different donors (one dot represents one donor) are indicated (n≥3 for 1-100 ng/mL and n=1 for 0.01-0.1 ng/mL). Each antibody was analyzed separately, comparing the contrast between (B) HSA and HSA-rocuronium or (C) the contrast between each HSA-roc concentration and the control medium without HSA-roc after mixed linear modeling and multiple-testing P-value adjustment. ***, $P < 0.001$. (**D**) Human neutrophil activation test using preformed immune complexes (IC) made of anti-rocuronium hIgG and HSA-rocuronium, with activation measured using (left) anti-CD11b staining, (middle) anti-CD62L staining and (right) percentage of unstimulated cells (n≥4). Effector-less "(NA)", heavy-chain $N_{297}A$ mutation, IgG antibodies were used as negative controls. Buffer condition is normalized to 100. (n=5). Mean ± standard deviation of different donors (dots) is indicated. In each panel, contrast between IgG1(NA) and IgG1 was compared for each antibody, after mixed linear modeling and multiple-testing P-value adjustment. ***, $P < 0.001$; **, $P < 0.01$; *, $P < 0.05$.

Figure 5: **IgE-mediated passive systemic anaphylaxis in hFcεRI-transgenic mice**. (**A**) Scheme of induction of passive systemic anaphylaxis in hFcεRI-transgenic mice, with (top) one or (bottom) two sensitizations. (**B-C**) Passive systemic anaphylaxis measured by changes in body temperature (ΔTemperature) in hFcεRI-transgenic mice sensitized (**B**) once with hIgE IP8 at indicated doses (n=3 independent experiments) or (**C**) once with 5 μg of hIgE IP2, IP8 or IP11 (n=6 independent experiments), and challenged with 2 μg HSA-rocuronium. (**D**) Passive systemic anaphylaxis in hFcεRI-transgenic mice sensitized with 40 μg of hIgE IP12 once at Time 0h and once at Time 24h, and challenged intravenously at Time 48h with 140 μg HSA-rocuronium (n=3). (B-D) Mean ±

standard deviation of the three mice per group are indicated. The effect of each antibody compared to the control was tested after mixed linear modeling and multiple-testing P-value adjustment. ***, $P < 0.001$; **, $P < 0.01$; *, $P < 0.05$. For D, each of the three injection effects were analyzed separately.

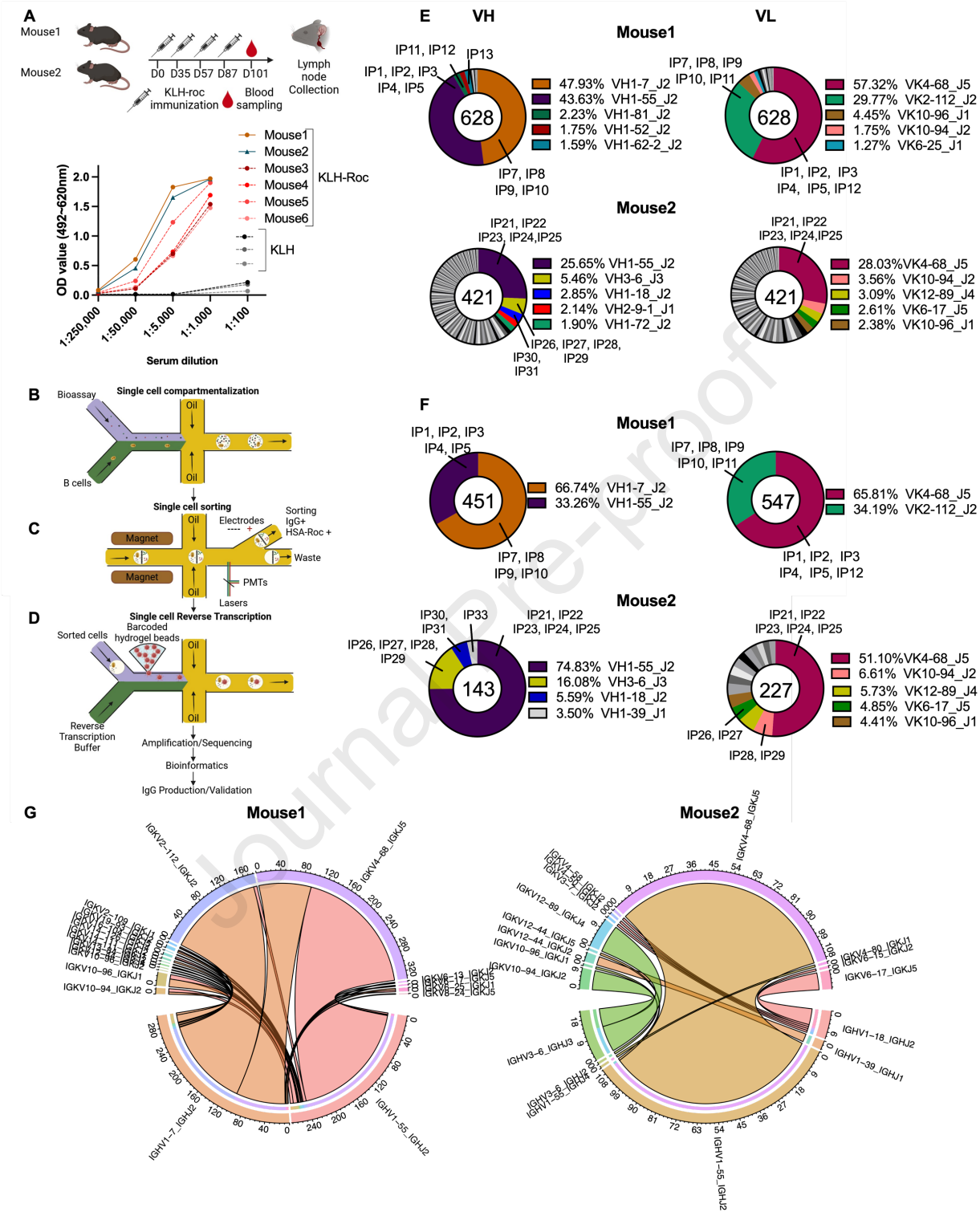

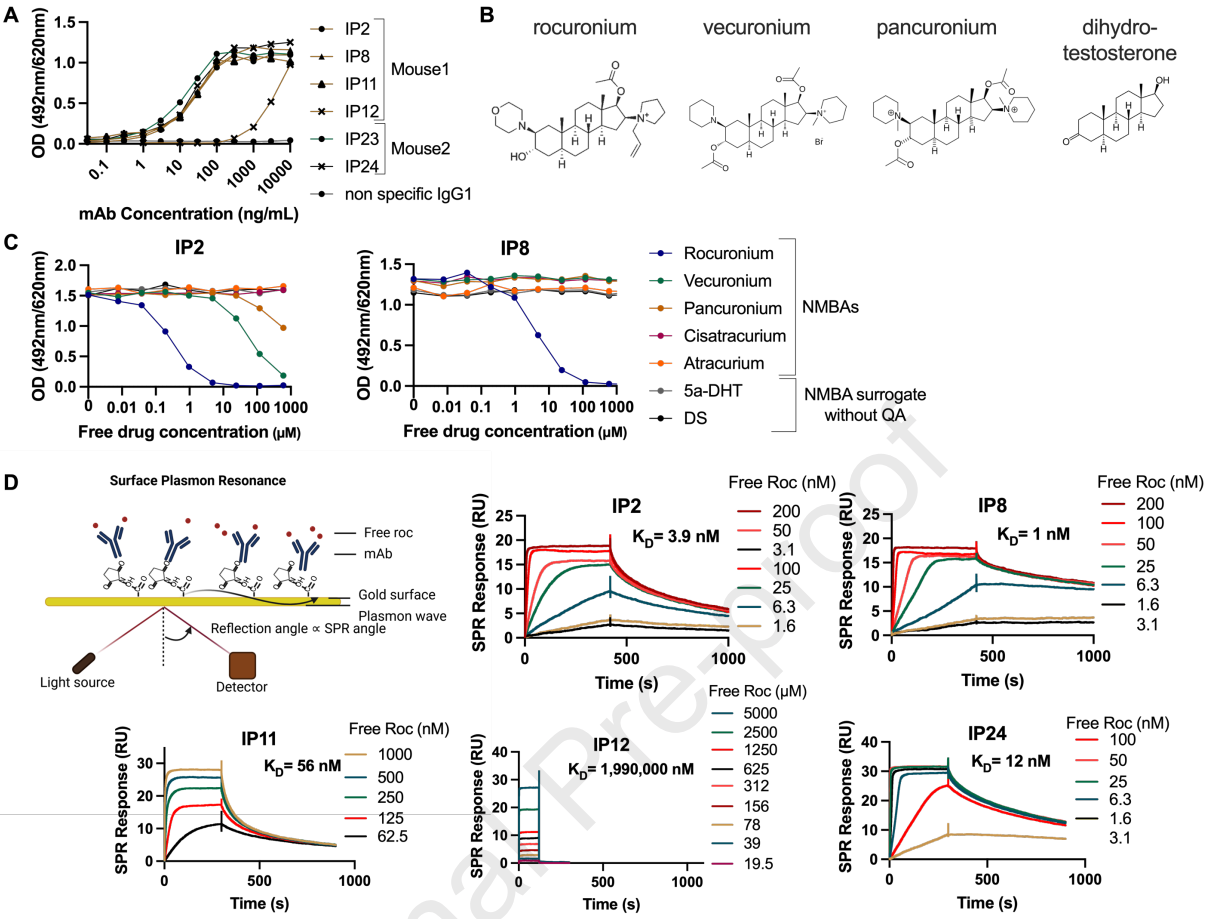

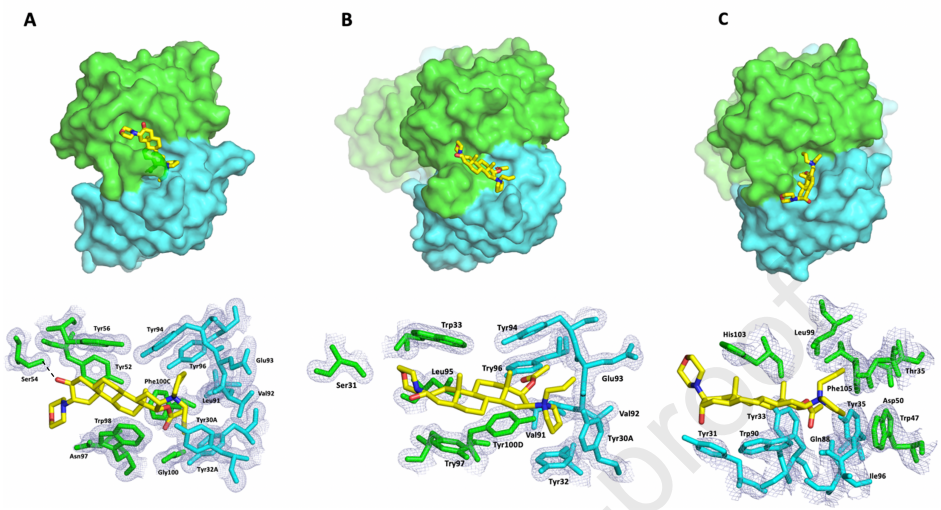

Figure 3: Crystal structures of mAbs in complex with rocuronium. Top: surface representation of co-crystal structures of rocuronium-specific scFv IP11 (A), Fab-IP8 (B) and Fab-IP2 (C). Bottom: superposition of the rocuronium and key residues of the binding site. The rocuronium molecule is shown in yellow and the antibody heavy chain and light chain are colored in green and cyan, respectively.

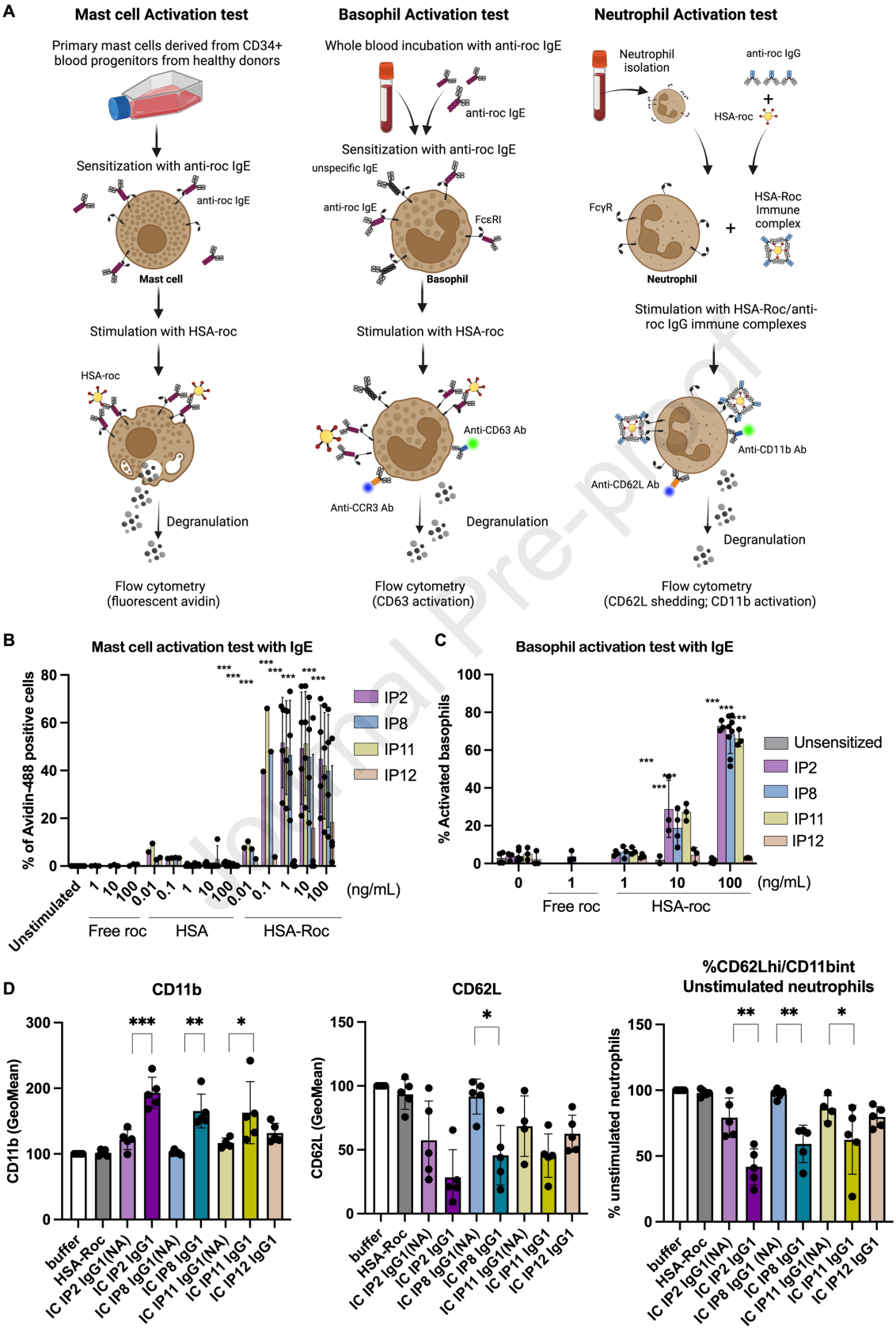
A
Mast cell Activation test
Primary mast cells derived from CD34+ blood progenitors from healthy donors
Sensitization with anti-roc IgE
anti-roc IgE
Mast cell
Stimulation with HSA-roc
HSA-roc
Degranulation
Flow cytometry (fluorescent avidin)
Basophil Activation test
Whole blood incubation with anti-roc IgE
anti-roc IgE
Sensitization with anti-roc IgE
unspecific IgE
anti-roc IgE
FcεRI
Basophil
Stimulation with HSA-roc
Anti-CD63 Ab
Anti-CCR3 Ab
Degranulation
Flow cytometry (CD63 activation)
Neutrophil Activation test
Neutrophil isolation
anti-roc IgG
HSA-roc
FcγR
HSA-Roc Immune complex
Neutrophil
Stimulation with HSA-Roc/anti-roc IgG immune complexes
Anti-CD11b Ab
Anti-CD62L Ab
Degranulation
Flow cytometry (CD62L shedding; CD11b activation)
B
Mast cell activation test with IgE
% of Avidin-488 positive cells
IP2
IP8
IP11
IP12
Unstimulated
(ng/mL)
Free roc
HSA
HSA-Roc
C
Basophil activation test with IgE
% Activated basophils
Unsensitized
IP2
IP8
IP11
IP12
(ng/mL)
Free roc
HSA-roc
D
CD11b
CD11b (GeoMean)
CD62L
CD62L (GeoMean)
%CD62Lhi/CD11bint Unstimulated neutrophils
% unstimulated neutrophils
buffer
HSA-Roc
IC IP2 IgG1(NA)
IC IP2 IgG1
IC IP8 IgG1(NA)
IC IP8 IgG1
IC IP11 IgG1(NA)
IC IP11 IgG1
IC IP12 IgG1